CrossMark

ORIGINAL PAPER

PDCD10 (CCM3) regulates brain endothelial barrier integrity in cerebral cavernous malformation type 3: role of CCM3-ERK1/2-cortactin cross-talk

Svetlana M. Stamatovic[1] · Nikola Sladojevic[1] · Richard F. Keep[2,3] · Anuska V. Andjelkovic[1,2]

Abstract Impairment of brain endothelial barrier integrity is critical for cerebral cavernous malformation (CCM) lesion development. The current study investigates changes in tight junction (TJ) complex organization when PDCD10 (CCM3) is mutated/depleted in human brain endothelial cells. Analysis of lesions with CCM3 mutation and brain endothelial cells transfected with CCM3 siRNA (CCM3-knockdown) showed little or no increase in TJ transmembrane and scaffolding proteins mRNA expression, but proteins levels were generally decreased. CCM3-knockdown cells had a redistribution of claudin-5 and occludin from the membrane to the cytosol with no alterations in protein turnover but with diminished protein–protein interactions with ZO-1 and ZO-1 interaction with the actin cytoskeleton. The most profound effect of CCM3 mutation/depletion was on an actin-binding protein, cortactin. CCM3 depletion caused cortactin Ser-phosphorylation, dissociation from ZO-1 and actin, redistribution to the cytosol and degradation. This affected cortical actin ring organization,

TJ complex stability and consequently barrier integrity, with constant hyperpermeability to inulin. A potential link between CCM3 depletion and altered cortactin was tonic activation of MAP kinase ERK1/2. ERK1/2 inhibition increased cortactin expression and incorporation into the TJ complex and improved barrier integrity. This study highlights the potential role of CCM3 in regulating TJ complex organization and brain endothelial barrier permeability.

Keywords CCM3 · Tight junction · Cortactin · Brain endothelial barrier · Permeability

Introduction

Cerebral cavernous malformations (CCM) are the most common type of brain vascular malformation. They are characterized by multiple or isolated vascular dilations/lesions located in any region within the CNS [16, 31]. Based on magnetic resonance imaging, CCM prevalence is 0.4–0.9 %, which represents 5–13 % of all vascular malformations. They occur equally in males and females, with a mean age at clinical presentation of 10–40 years [8, 49]. Nearly, 50–80 % of patients with CCM have the sporadic form (solitary lesion) with a negative family history, while 8–19 % are inherited (multiple lesions) [3]. Patients with CCM are subject to hemorrhagic stroke, seizures, epilepsy, migraine-like headaches and other neurological sequelae [1, 2, 13, 31, 49].

In both inherited (CCM1, CCM2 and CCM3) and spontaneous CCM (sCCM), lesions are grossly defined as enlarged and thin-walled vascular sinusoids lined by a thin endothelium without intervening brain parenchyma. These sinusoidal structures can be thrombosed as well as surrounded by hemosiderin deposits and gliosis resulting

✉ Anuska V. Andjelkovic
anuskaa@med.umich.edu

1 Department of Pathology, University of Michigan, Medical School, 7520A MSRB I, 1150 W Medical Center Dr, Ann Arbor, MI 48109-5602, USA

2 Department of Neurosurgery, University of Michigan, Medical School, R5018 BSRB, 109 Zina Pitcher Place, Ann Arbor, MI 48109-2200, USA

3 Department of Molecular & Integrative Physiology, University of Michigan, Medical School, R5018 BSRB, 109 Zina Pitcher Place, Ann Arbor, MI 48109-2200, USA

from prior hemorrhage [6, 14, 16, 72]. Histologically, CCM have poorly formed tight junctions (TJs) between adjacent endothelial cells, with gaps often noted between individual cells [5, 6, 50]. Pericytes are scant and no astrocytic foot processes and no normal nervous tissues are present within the lesions [34, 52, 61, 63]. A common finding of all CCM lesions is increased vascular permeability due to disorganization of the TJ complex, a critical structure regulating brain endothelial barrier tightness [6, 23, 39, 73].

In recent years, significant progress has been made in understanding CCM pathogenesis. Deletion or functional mutations in three separate genes have been identified in association with familial CCM: Krit1 (CCM1), MGC4607 (CCM2) and PDCD10 (CCM3). These proteins appear to interact with cytoskeletal and interendothelial cell junction proteins, generating a typical pathological substrate in CCM: altered microvascular and blood–brain barrier (BBB) permeability [5, 32, 41, 45, 56]. In CCM1 mutations, vascular hyperpermeability results from a dysfunctional Krit/Rap1 pathway leading to inadequate TJ assembly. CCM2 mutations cause overactive RhoA/ROCK signaling, a pathway responsible for cytoskeletal remodeling and endothelial permeability [4, 17, 33, 59]. CCM3 (PDCD10) is a pleiotropic molecule involved in a variety of signaling events associated with angiogenesis, barrier permeability, apoptosis, oxidative metabolism and Golgi complex polarization [9, 19, 27, 74]. Although CCM3 mutations cause early and severe brain vascular lesions, the target of the mutation is still uncertain [12].

CCM3 resides within two complexes, which define its cell function, with CCM1/CCM2 (20 %) and as part of STRIPAK complex (80 %) [21, 22, 27]. Based on experimental and clinical data, CCM1-3 proteins are physically associated in order of CCM1–CCM2 and CCM2–CCM3, and the complex is required for correct protein localization at endothelial cell–cell junctions, vascular tubular and network stability as well as cell survival and proliferation [10, 21, 22]. In particular, CCM2–CCM3 interaction is indicated as maintaining stability of CCM3 and CCM2 proteins and protection from proteasomal degradation and normal endothelial cell network formation [10]. A recent proteomic study found that CCM3 in the STRIPAK complex established mutually exclusive interactions with PIP2A, germinal center kinases III (Stk24, Stk25, Mst4) and cortical actin-binding protein 2 (CTTNBP2). It may participate in regulating VEGFR2 receptor stability, PIP2A enzyme association with membrane phospholipids like PIP2 and PIP3, apoptosis and endothelial cell growth [9, 19, 21, 22, 27, 60]. CCM3 localization and molecular interaction in both complexes are considered critical for understanding CCM3 function, potential overlap between CCM2 and CCM3 pathology (due to CCM2 and CCM3 direct interaction) and differences from CCM1 and CCM2 pathways

(RhoA, Cdc42 signaling and actin rearrangement) [10, 21, 66, 74]. How CCM3 regulate the TJ complex assembly and permeability, which target and signaling pathways are critical for development of CCM3 lesion is still awaits clarification. The present study addresses the role of CCM3 in regulating BBB integrity and defines potential targets of CCM3 action at the TJ complex.

Materials and methods

Brain tissue

Human brain CCM tissue samples were obtained from the Angioma Alliance Biobank (http://www.angiomaalliance.org, Norfolk, VA, USA). The study includes five clinically and genotypically analyzed CCM lesions and 4 normal brain controls. Cases included patients with CCM3 mutation (CCM3 c.474+1G>A) and the sporadic form of CCM without CCM1, CCM2 and CCM3 mutations. According to medical records, brain tissue was collected from patients with single and multiple CCM lesions after surgical resection, with clinical symptoms, which included headache, seizures, poor vision, behavioral changes, history of hemorrhagic stroke and no history of gamma knife radiosurgery. Control brain slides were obtained from ProSci Incorporated (Poway, CA, USA) and had no cerebrovascular malformations. Details of the brain samples utilized in this study are included in Supplemental Table 1. Ethical approval for these studies was obtained from the Institution Review Board, University of Michigan Medical School. Fresh frozen tissue was fixed with 4 % paraformaldehyde and cryoprotected with 30 % of sucrose and cut at 10 µm while formalin fixed. Paraffin-embedded brain tissue was cut at 4 µm. CCM lesions and human brain tissue were used for immunohistochemistry, PCR array and Western blot analysis.

Laser capture microdissection (LCM)

Tissue sections from CCM3 lesions and control brain sections were mounted on pen slides for LCM. Sections were deparaffinized by incubations in xylene for 2.5 and 1.5 min and rehydrated by consecutive incubations in 100 % ethanol, 70 % ethanol and water, each for 1 min. Samples were stained with Mayer's hematoxylin and briefly washed with diethyl pyrocarbonate-treated tap water, air-dried and stored at 4 °C. Endothelial cells from lesion and small caliber brain blood vessels (diameter ~10 µm) were dissected using a Veritas LCM system (Arcturus Engineering Inc). Microdissected material (~500 brain endothelial cells) was collected directly, taking care to avoid contamination with surrounding glial cell components, by placing specific

polymer film mounted on optically transparent caps (Cap-Sure, Arcturus Engineering) on the section. The caps with captured endothelial cells were mixed with RNA extraction buffer (Arcturus Engineering) and samples were prepared following the manufacturer's instructions. For Western blot analyses, dissected tissue/brain endothelial cells was prepared by a two-step digestion protocol using 0.1 M Tris–HCl, pH 8.0, 0.1 M DTT, 0.5 % (w/v) polyethylene glycol 20,000, 4 % SDS and 8 M in 0.1 M Tris–HCl pH 8.5, described by Wisniewski and Mann [71].

Cell culture

Human brain endothelial cells (HBMEC) were obtained from ScienCell (Carlsbad, CA, USA). Cells were plated on fibronectin-coated flasks and grown in endothelial cell medium, 5 % fetal bovine serum, 1 % endothelial cells growth supplement and 1 % penicillin/streptomycin solution in 5 % CO_2/95 % air at 37 °C. In all experiments, cells were used at 1st or 2nd passage.

Cell transfection

Optimal inhibition of CCM3 was achieved after transfection with a cocktail of three siRNA oligonucleotides targeting three different regions of the CCM3 (PDCD10) gene (siRNA ID 22175, 22176 and 22177; Life Technology). Control (mock) cells were transfected with Silencer Select Negative control siRNA (sicontrol #1). Inhibition of cortactin (CTTN) was achieved after transfection with either human CTTNshRNA or a cocktail of three unique CTTN 27mer siRNA duplexes (OriGene Technologies, Inc). For rescue experiments, human CCM3 (PDCD10) and cortactin cDNA were purchased from OriGene Technologies, Inc. In general, HBMEC were transfected with either annealed siRNAs, shRNA or cDNA using Lipofectamine 2000 (Applied Biosystems) transfection agent and were subcultured 24 h later. Cells were used 24 h later for experiments. The efficiency of the transient depletion was tested 1–7 days after transfection by Western blot analysis (Supplemental Fig. 1). Cell viability was measured after transfection (0–72 h) and after retransfection 3 days later using a CellTiter 96® Non-Radioactive Cell Proliferation Assay (Promega). Proliferative ability and apoptosis were examined in CCM3-knockdown cells (CCM3-KD) by BrdU Cell Proliferation Assay (Cell signaling Technology) and Caspase-3 Activity Assays (Life Technology), respectively.

Cell treatment

Cells were exposed to inhibitors for 0–24 h. Control cells were exposed to assay media (DMEM) alone. The following inhibitors (all from Sigma-Aldrich) were used: 5 µg/ml cycloheximide, 10 µM PD98059, 25 µg/ml Leupeptin, 10 µM MG-132 and 50 µM E3 ubiquitin ligase inhibitor (SMER3). Cell viability assays were performed to exclude possible toxic effects and only cells with 98 % of viability were used in experiments. The effects of treatment and inhibitors were evaluated by Western blot.

Immunofluorescence and quantification of fluorescence intensity

Paraffin-embedded brain tissue was dewaxed and rehydrated through xylene and a series of alcohols (100, 95, 70 and 50 %). Antigen retrieval was performed by boiling slides in 10 mM sodium citrate buffer (pH 6.0) for 10 min, followed by cooling and washing in PBS (pH 7.2). Cell samples washed in PBS and fixed in 4 % paraformaldehyde. For immunofluorescence staining, brain and cell samples were preincubated in blocking solution containing 5 % normal goat serum and 0.05 % Triton 100X (Sigma Aldrich) in PBS. Samples were then incubated overnight at 4 °C with the following primary antibodies: anti-CD31, Ve-cadherin and β-catenin (BD Bioscience) JAM-A (R&D System), claudin-5-Alexa-Fluor 488 conjugated, occludin-Texas Red, ZO-1-Alexa Fluor 594, claudin-1-Alexa Flour 488, claudin-3, claudin-1 (Life Science Technology). Reactions were visualized by fluorescein- or Texas Red-conjugated anti-mouse and/or anti-rabbit antibodies. All samples were viewed on a confocal laser-scanning microscope (LSM 510, Zeiss). The actin cytoskeleton in cell cultures was visualized with phalloidin-Alexa 568 (Life Science Technology).

To measure the fluorescent intensity by tissue array, three sections per CCM case and control slides were chosen and on each histological slide ten spots were randomly selected [24]. Images (30 images per each staining) for quantitative florescence analysis were acquired using a Zeiss LSM META 510 laser-scanning microscope with sequential mode to avoid interference between channels and saturation. Contrast, brightness and the pinhole were held constant. Analysis was done in ImageJ software by outlining the endothelial cells (CD31+ve staining) in the lesion or blood vessels in controls in each image and the fluorescence intensity in the enclosed area was measured. Background intensity was subtracted from the fluorescence intensity [24].

Co-immunoprecipitation and Western blotting

For co-immunoprecipitation, cells were washed with PBS and lysed in 1 ml RIPA buffer (50 mM Tris–HCl, pH8.0, 150 mM NaCl, 1 % Triton X-100, 0.5 % Na-deoxycholate, 0.1 % SDS, 1 mM EDTA, 1 mM Na_3VO_4, 10 µg/ml

aprotinin, 10 µg/ml leupeptin, and phosphatase inhibitor cocktail; Sigma Aldrich). Lysates were centrifuged at 10,000 rpm and exposed to anti-ZO-1, -cortactin or -β-actin antibody for 1 h. RIPA buffer equilibrated EZviewRed protein G affinity Gel beads (Sigma Aldrich) was then added to the lysate–antibody mixture and incubated for 1 h at 4 °C. The beads were then extensively washed with RIPA buffer and bound protein eluted by adding 2× sample buffer and boiling at 100 °C. Samples were examined by Western blot using anti-claudin-5, -occludin or -JAM-A antibodies.

For Western blots, formalin-fixed and paraffin-embedded CCM3 and control brain tissue samples were prepared by a two-step digestion protocol [71]. Western blotting was performed using: anti-JAM-A (R&D Systems), anti-claudin-1, -3 and -5, and -occludin (Life Science Technology), anti-ZO-1, ubiquitin, -cortactin, β-actin (Cell Signaling Technology), anti-CD31, Ve-cadherin and β-catenin (BD Bioscience) antibodies. Immunoblots were exposed to secondary antibodies either anti-mouse or anti-rabbit IgG Fc-HRP (Abcam) or mouse anti-rabbit light chain HRP antibody (Millipore) and visualized with a chemiluminescent HRP substrate kit and analyzed using Image J software.

Cell fractionation analysis of tight junctions

The cellular distribution of TJ proteins was analyzed using a ProteoExtract Subcellular Proteome Extraction kit (Calbiochem). Membrane, cytosolic, cytoskeletal and nuclear fractions were separated. Specificity of fractions was confirmed using anti-cytochrome P450 reductase (membrane fraction), anti-calpain (cytosolic fraction) and anti-vimentin (actin cytoskeletal fraction) antibodies [58]. For "total cell lysate" samples, cells were washed in PBS, scraped and rinsed in 1 ml of the lysis buffer (25 mM Tris–HCl pH 7.4 with 150 mM NaCl, 0.1 % SDS, 1 % Triton X-100, and 1 % deoxycholate). Isolated fractions were analyzed by Western blotting.

In some experiments, the actin cytoskeletal fraction was further fractionated into a high-density Triton-insoluble fraction, for separation of the cytoplasmic actin cytoskeleton, and a low-density Triton-insoluble fraction, for separation of the membrane-associated cytoskeleton. Briefly, cells were washed with ice-cold PBS and incubated with lysis buffer (25 mM Tris–HCl pH 7.4 with 150 mM NaCl, 1 % Triton X-100, 10 µg aprotinin, 10 µg pepstatin-A, 1 mM vanadate and 1 mM PMSF). Samples were then centrifuged at 15,600g for 5 min at 4 °C and the sediment (high-density actin cytoskeleton) was collected while the supernatant was further centrifuged at 100,000g for 4 h at 4 °C with the resulting sediment representing the low-density membrane cytoskeleton [43]. Both collected sediments were resuspended in 300 µl of lysis buffer; protein content

was determined by Bradford protein assay (Thermo Scientific) and mixed with Pierce LDS Sample Buffer (Thermo Scientific).

Real-time RT-PCR

Microvessels from CCM3 lesions and control brain tissue were collected using LCM. Total RNA from the microvessels and hBMEC was prepared using TRIZOL (Life Technologies). Single-strand cDNA was synthesized using RT^2 first strand kit (QIAGEN). Real-Time PCR was performed for cortactin proteins using SABioscience primers (QIAGEN). Analysis of junction protein mRNA expression in CCM3, sCCM lesion and control brain tissue was done using Cell Junction PCR array (QIAGEN). The expression pattern of junction protein mRNA was evaluated using software provided by the manufacturer.

Brain endothelial cell monolayer permeability

The permeability of brain endothelial cell monolayers to FITC-inulin (5 kDa, Sigma Aldrich), Dextran Cascade Blue (20 kDa) and Dextran Texas Red (40 kDa, Life Science Technology) were measured as described previously [26, 58]. Briefly, hBMEC were plated on a Transwell Dual chamber system at a density of 1×10^5 and transfected with CCM3 or cortactin siRNA and corresponding control (nonsense siRNA). Monolayer permeability was measured daily from 1–7 days. Permeability experiments were initiated by adding a cocktail of both tracers (10 µg/ml), in phenol red free DMEM (Life Science Technology) in the donor (apical) chamber. Media were sampled after 30 min from the receiving chamber. Fluorescence intensity was determined by fluorescent reader (Tecam) and concentration determined from a standard curve. The permeability (P; cm/min) of the monolayer for each time points (days) (T) was calculated using the following equation:

$$P = \frac{(C(B)_T - C(B)) \times V(B) \times 2}{(C(A) + C(A)_T) \times A}$$

where C(B) and C(B)$_T$ are, respectively, the concentrations of tracer in the basal chamber at the start and at the end of the time interval of 30 min (in µg/ml), and V(B) is the volume of the basal chamber (in ml). C(A) and C(A)$_T$ are, respectively, the tracer concentrations in the apical (donor) chamber at the start and at the end of the time interval of 30 min (in µg/ml) and A is the area of the filter (cm^2) [26, 58]. Cell density was evaluated after tracer permeability measurement by MTS assay (Promega). The number of cells was determined from an established standard curve of cell concentration vs. formazan absorbance. The examined monolayers had approximately 1.5×10^5 cells/well.

Kinase activation assay

The functional assay for ERK1/2 (Life Technology), RhoA (Cytoskeleton), and ROCK (Cell Biolabs, Inc.) activity was performed in total cell lysates, according to the manufacturer's instruction.

Statistical analysis

Unpaired Student's *t* test and one-way analysis of variance (ANOVA) were used to test group level differences. For post hoc comparisons, Bonferroni's tests were applied. A probability value <0.05 was regarded as statistically significant. For assessment of junction protein level after normalization over the time period after addition of cycloheximide was analyzed by nonlinear regression with GraphPad Prism assuming one-phase exponential decay.

Results

Tight junction and brain endothelial barrier properties in CCM3 lesions

Since CCM lesions have different pathological substrata for their development, we classified the CCM cases based on confirmed presence CCM gene mutations. The analysis focused on junction protein expression in two types of lesion: (a) CCM3 lesions, which had a confirmed CCM3 mutation (CCM3 c.474+1G>A) and no CCM3 protein present in endothelial cells along the lesion, and (b) sporadic CCM (sCCM) lesions that had a characteristic mulberry-like structure, no CCM3, CCM1 or CCM2 gene mutations and CCM3 protein present in endothelial cells (Supplemental Fig. 1a).

Junction protein mRNA expression was analyzed in brain endothelial cells in CCM3, sCCM lesion and control brain tissue by laser capture microdissection. There were increases in the mRNA expression of transmembrane (claudin-5, occludin, JAM-A, JAM-B and JAM-C), scaffolding [ZO-1, ZO-2, Afadin-6 (Af-6), nectin], actin-binding (VASP, cortactin) and adherens junction (Ve-cadherin, α, β-cateinin and p120) proteins in both CCM3 and sCCM lesions compared to control. In particular, there were sixtenfold increases in the transmembrane TJ proteins claudin-1 and claudin-3 in both CCM3 and sCCM lesions, due to very low mRNA expression of claudin-1 and -3 in control microvessels (Fig. 1a).

The upregulation in tight and adherens junction (AdJ) protein mRNA expression was not, however, associated with increased protein expression as assessed by three techniques. Analyses of brain endothelial cells in control, CCM3 and sCCM by tissue array showed significant

down-regulation in two transmembrane TJ proteins, claudin-5 and occludin, the scaffolding protein ZO-1, as well as two actin-binding proteins and components of the cortical actin ring, cortactin and VASP ($p < 0.001$). In particular, there was a very marked reduction in cortactin in CCM3 lesions compared with controls and sCCM lesions (Fig. 1b). The AdJ proteins, Ve-cadherin, β-catenin and α-catenin showed a slight but not significant down-regulation in both CCM3 and sCCM lesions (Fig. 1b).

The pattern of junction protein expression and localization was further analyzed in tissue by immunofluorescence and by LCM with Western blot. Initial immunostaining with an endothelial cell marker, CD31, showed that all cystic formations in both CCM3 and sCCM lesions were layered with CD31+ve endothelial cells while there was very low or absent expression of CD31 in the surrounding tissue (Fig. 2a). The CD31+ endothelial cells in the lesions had noticeable alterations in the pattern of immunostaining for the transmembrane TJ proteins, claudin-5 and occludin. Claudin-5 had a fragmented pattern of staining with areas of complete loss in CCM3 lesions and, to a lesser degree, in sCCM lesions compared with control (continuous staining around the vessel lumen). A similar pattern was also found for occludin immunostaining in both lesion types and there was notable expression in "surrounding" tissue (Fig. 2a). By Western blot, both claudin-5 and occludin had marked decreases in protein expression, particularly in CCM3 lesions. In contrast, staining of JAM-A, another transmembrane TJ protein, was similar in control, CCM3 and sCCM vessels with continuous staining along the lumen and a slight alteration (increase) in protein expression in sCCM lesions (Fig. 2a, b). Immunostaining for ZO-1 in the endothelial cells of CCM3 lesions was mostly decreased and punctate. There were less pronounced changes in sCCM lesions (Fig. 2a, b). Regarding AdJ proteins, Ve-cadherin expression and localization in CCM3 lesions varied from a fragmented pattern to absence of any staining in some cystic formations, while β-catenin did not show any specific changes in presence or localization in CCM lesions. However, total Ve-cadherin and β-catenin protein expression was not significantly changed in CCM3 lesions, while there was a slightly higher expression in sCCM lesions (Ve-cadherin; $p < 0.05$; Fig. 2b), although such a difference was not found by tissue array (Fig. 1b). Analysis of cortactin distribution showed significant loss of endothelial staining along cystic formations, particularly in CCM3 lesions and to a lesser degree with sCCM. Sporadic cortactin +ve cells were found in surrounding tissue.

Taken together, the above results indicate that CCM3 and sCCM lesions have significant alterations in junction protein expression and localization at the brain endothelial barrier. Three techniques for examining protein expression all found that there are decreased levels of key
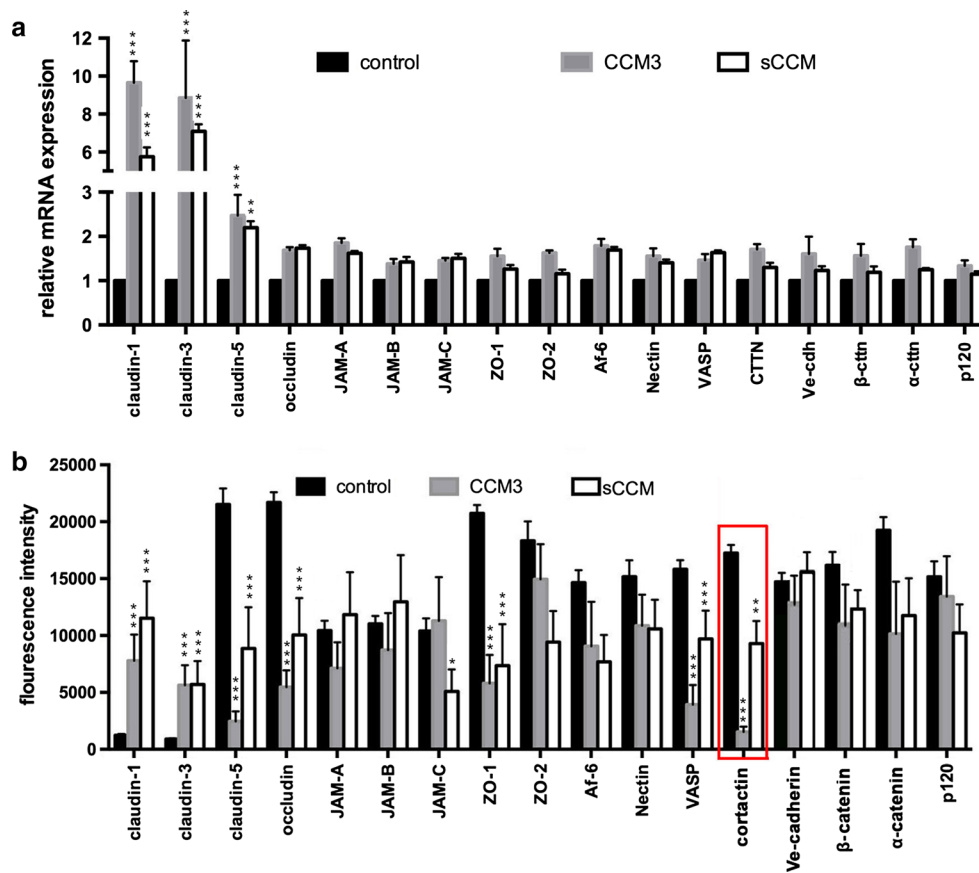
Fig. 1 **a** mRNA microarray and **b** tissue array for junctional proteins present in brain tissue of control (age and gender matched), CCM3 lesion (case with CCM3 c.474+1G>A mutation) and sCCM (cases with sporadic form of CCM). For the mRNA microarray array (**a**), data represent relative mRNA expression, while the tissue array (**b**) is total florescence intensity of 30 analyzed spots on CCM lesions or blood vessels in controls (see "Materials and methods" section). Values are mean ± SD, $n = 3$ control brain, $n = 2$ CCM3 cases, $n = 3$ sporadic CCM cases (sCCM). *$p < 0.05$, **$p < 0.01$ and ***$p < 0.001$ compared to control samples

transmembrane TJ proteins, claudin-5 and occludin, diminished ZO-1 expression and most profoundly reductions in actin-binding proteins. In particular, cortactin expression is down-regulated in CCM3 lesions.

Tight junction and brain endothelial barrier properties with CCM3 knockdown

To analyze the role of CCM3 in regulating endothelial barrier integrity, we generated CCM3-depleted cells by transfecting hBMEC with CCM3 siRNA. Transient transfection and knockdown of CCM3 were optimized to induce prolonged (7 days) depletion of CCM3 mRNA (>80 %) and protein (>65 %) by re-transfecting after 3 days with minimal toxic effects (Supplement Fig. 1b, c and d). Loss of CCM3 did not significantly alter the proliferative capacity of the hBMEC (Supplement Fig. 1d). Prolonged depletion of CCM3 was important as, in vitro, brain endothelial barrier integrity manifested by barrier impermeability and complete TJ complex formation occurred on day 5–7 after

initial plating. Thus, the generated CCM3 knockdown cells (CCM3-KD) represent a good system to define whether, when and how CCM3 affects the brain endothelial TJ complex.

Brain endothelial barrier integrity in control and CCM3-KD cells was assessed by in vitro permeability assay using different sized tracers, sodium fluorescein (376 Da), FITC-labeled inulin (5 kDa), dextran-Texas red (20 and 40 kDa) between 1 and 7 days after initial plating. In control cells, the permeabilities of each tracer decreased progressively with time, reaching very low levels by ~day 5 (Fig. 3a). In CCM3-KD cells, there was a decline in the permeability to 40 and 20 kDa dextran with time, but this was slower than in control cells and incomplete by 7 days. Thus, compared to control monolayers, CCM3-KD cell monolayers were significantly hyperpermeable at days 3–7 for 40 kDa dextran and days 2–7 for 20 kDa dextran (Fig. 3a). In addition, for the small molecular weight tracer inulin (5 kDa), the permeability of the CCM3-KD monolayers did not decrease with time and were hyperpermeable compared to
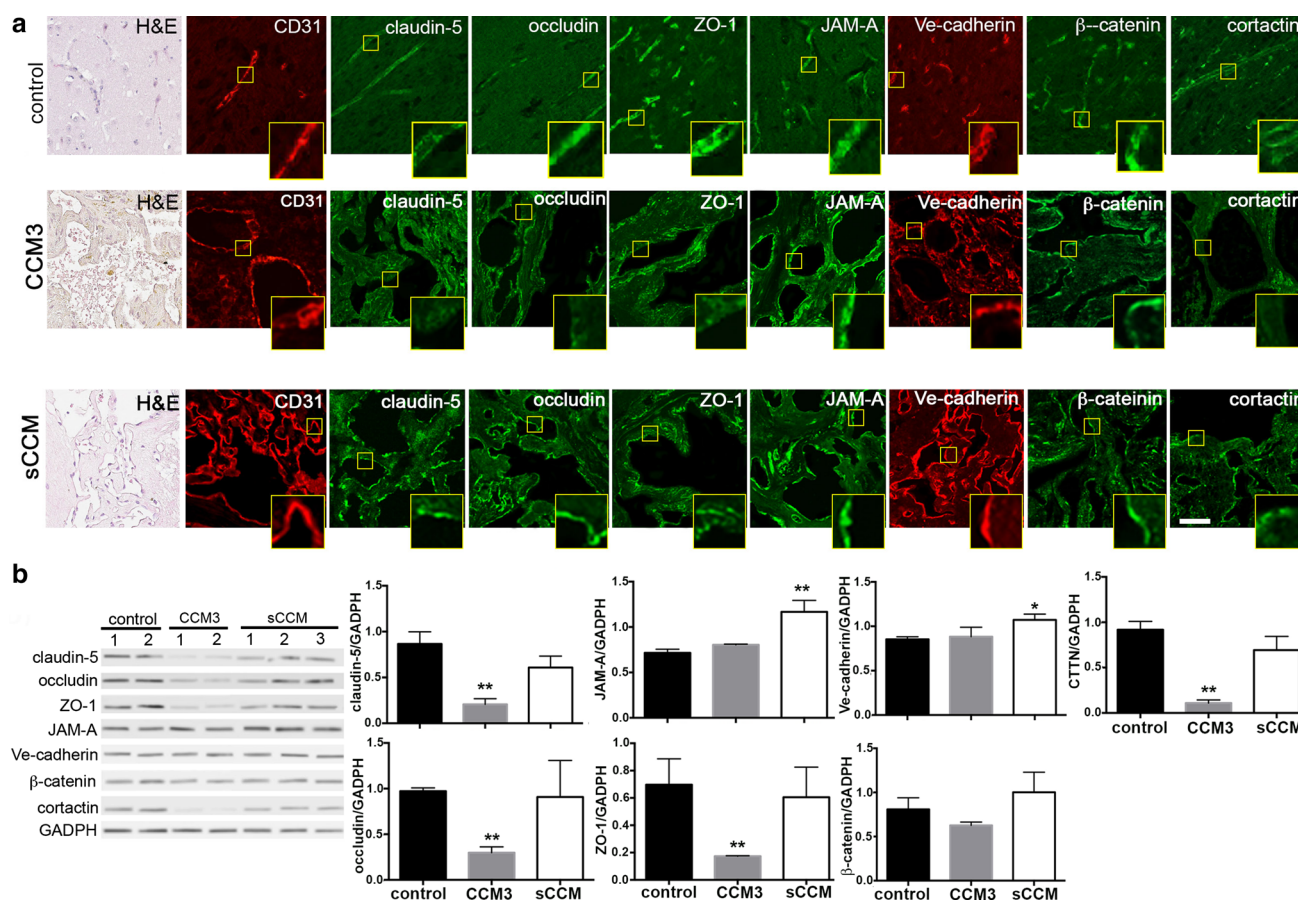
Fig. 2 a Representative immunofluorescent images of junctional protein expression in CCM3 and sCCM brain lesions. Mag. ×10 and ×20 (H&E control, CCM3 and sCCM). *Scale bar* 20 μm. **b** Representative images of Western blot analysis of TJ proteins (claudin-5, occludin, ZO-1 and JAM-A), AdJ proteins (Ve-cadherin and β-catenin) and an actin-binding protein, cortactin in all CCM3 and sCCM laser capture microdissection samples. Relative protein expression in control, CCM3 and sCCM samples was determined by semi-quantitative analysis. Values are mean ± SD, $n = 3$ control brain, $n = 2$ CCM3 cases, $n = 3$ sporadic CCM cases (sCCM). $*p < 0.05$ and $**p < 0.01$ compared to control samples

control cells from day 2 to 7 (all $p < 0.001$; Fig. 3a). A similar difference in barrier permeability between CCM3-KD and control cells was found for another small molecular tracer, sodium fluorescein (376 Da; data not shown). The differences in barrier permeability with CCM3-KD were not due to differences in endothelial cell density, which were not significantly different from controls from day 1 to 7 (Fig. 3a). Thus, CCM3 depletion in brain endothelial cells caused increased barrier permeability for a variety of molecular weight tracers, with particularly marked effects on inulin.

We further analyzed the TJ complex as a potential reason for the increased barrier permeability with CCM3-KD. The expression pattern of TJ protein was examined at the mRNA and protein levels. CCM3 knockdown did not significantly affect claudin-5, occludin, JAM-A and ZO-1 mRNA expression (Fig. 3b). However, there was reduced protein expression of the transmembrane TJ proteins,

claudin-5 and occludin (but not JAM-A) and the scaffolding protein ZO-1 at the time when the persistent barrier permeability to the tracer 20 kDa dextran was established, 5 days after initial plating (Fig. 3b).

Due to these alterations in TJ protein content in CCM3-KD cells, we examined whether CCM3 decreases the half-life of TJ proteins using the protein synthesis inhibitor cycloheximide (CXD). Brain endothelial cells were transfected with CCM3 or control nonsense siRNA and then treated with CXD for an additional 3–24 h and TJ protein levels analyzed by Western blot. At each time interval, the effect of CXD on TJ protein levels did not differ between control and CCM3-KD cells (Fig. 3c).

Because total protein expression is not a sufficient indicator of TJ complex organization, further analysis focused on the localization and interactions of transmembrane and scaffolding TJ proteins with CCM3 loss. Cell fractionation indicated that transmembrane TJ proteins, claudin-5,
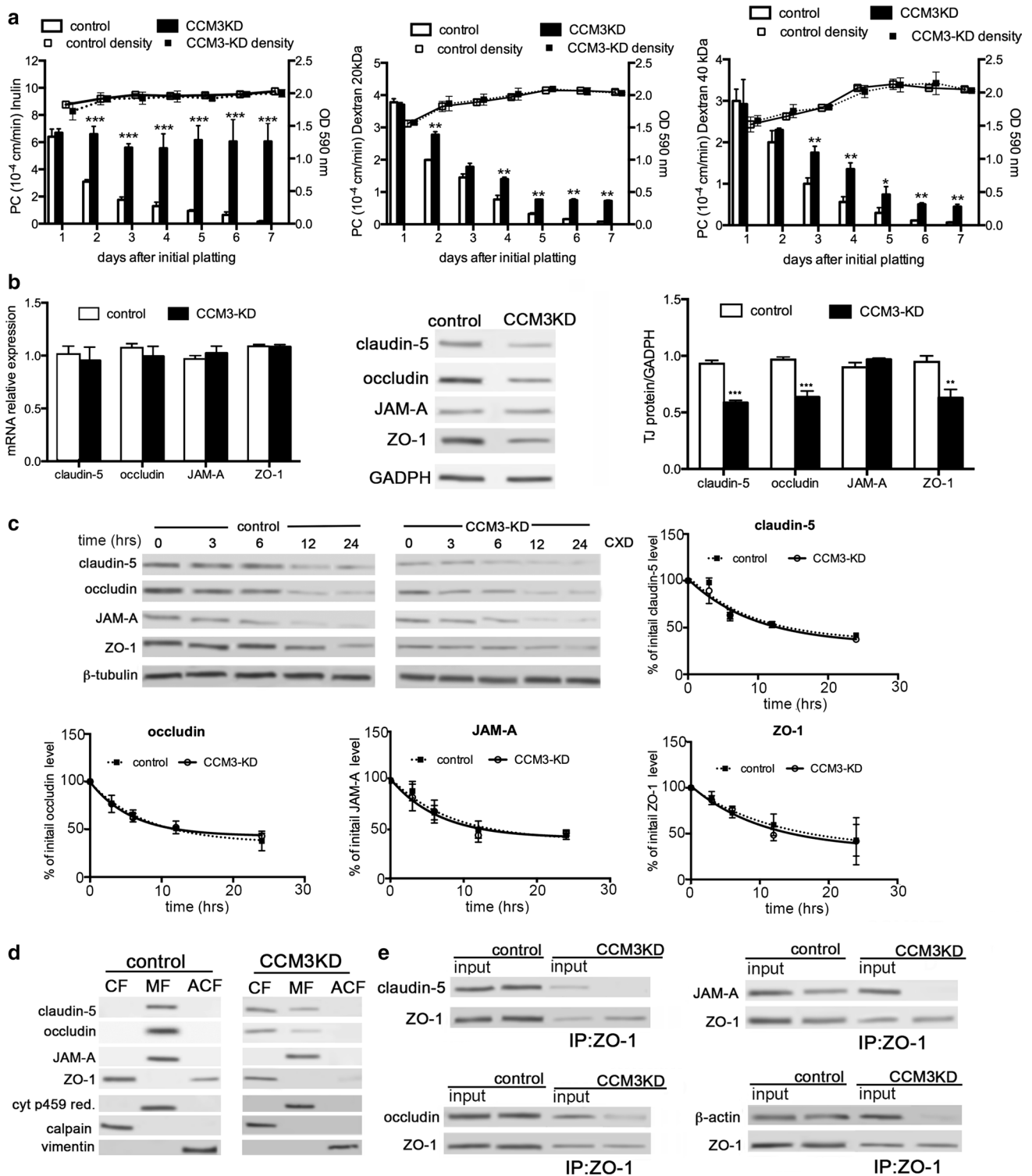
occludin and JAM-A, were predominantly localized in the membrane fraction in control cells while in CCM3-KD cells claudin-5 and occludin redistributed to the cytosol fraction. The scaffolding protein ZO-1 showed slight displacement in CCM3-KD cells with loss from the actin cytoskeleton fraction (ACF; Fig. 3d). However, analysis of TJ protein interactions, which are key for functionally active TJ complexes, indicated TJ disorganization. Co-immunoprecipitation with Western blotting indicated a loss of interaction/colocalization between the scaffolding protein ZO-1 and the transmembrane TJ proteins claudin-5, occludin and JAM-A in CCM3-KD cells compared to control cells (Fig. 3e). In

◀ **Fig. 3** **a** Permeability coefficient of brain endothelial monolayers for FITC-inulin (5 kDa), Cascade Blue-dextran (20 kDa) and Texas red-dextran (40 kDa) in control (scrambled siRNA) and CCM3-KD (CCM3 siRNA) transfected cells measured daily from 1 to 7 days after initial plating. Data represent mean ± SD for $n = 5$ independent, experiments. $*p < 0.05$, $**p < 0.01$ and $***p < 0.001$ comparing control and CCM3-KD cells. The total cell density in all experimental groups was assessed after each permeability measurement by MTT assay and is presented as the measured OD value for formazan. Note that there are no significant changes in density of cells (1–1.5×10^5 cells/well) over the time period of 1–7 days or between control and CCM3-KD groups. **b** Real-time RT-PCR and Western blot analysis of claudin-5, occludin, JAM-A and ZO-1 expression in control and CCM3-KD (siRNA) cells 7 days after initial plating. Data represent mean ± SD, $n = 3$; $**p < 0.01$ and $***p < 0.001$ comparing control and CCM3-KD cells. Western blot image is one of three independent experiments. GAPDH is an internal control. **c** TJ protein (claudin-5, occludin, JAM-A and ZO-1) turnover rate was analyzed following treatment with cycloheximide in CCM3-KD and control cells. Semi-quantitative densitometry for TJ protein was performed and normalized to β-tubulin as an internal control in three independent experiments. Cycloheximide (CXD) was added for 0–24 h in concentration of 5 µg/ml. Time point 0 is start for CXD treatment and for control and CCM3-KD cells was taken as 100 % of certain protein expression. The half-life of the proteins was: claudin-5, control cells = 6.4 h ($R^2 = 0.902$), CCM3-KD cells = 6.7 h ($R^2 = 0.929$). Occludin, control = 5.5 h ($R^2 = 0.968$) and CCM3-KD = 4.0 h ($R^2 = 0.960$). ZO-1, control = 8.8 h ($R^2 = 0.883$) and CCM3-KD = 7.4 h ($R^2 = 0.845$). JAM-A, control = 5.6 h ($R^2 = 0.923$) and CCM3-KD = 4.6 h ($R^2 = 0.889$), $n = 3$ independent experiments. There were no significant differences in TJ protein turnover between control and CCM3-KD cells. **d** Cell fractionation and Western blot analysis of claudin-5, occludin, JAM-A and ZO-1 distribution in CCM3-KD and control cells showed an increased accumulation of claudin-5 and occludin in the cytosol fraction (CF, TritonX-100 soluble fraction) in CCM3-KD cells compared to control cells where almost all of those proteins was in the membrane fraction (MF, TritonX-100 insoluble). ZO-1 was distributed in the cytosol fraction (CF, TritonX-100 soluble) and actin cytoskeleton fraction (ACF, TritonX-100 insoluble) in control cells, while in CCM3-KD cells was predominantly present in the CF. Blots represent one of three successful experiments. Cytochrome P450 reductase, calpain and vimentin represent the markers for membrane, cytosol and actin cytoskeleton fractions. **e** Co-immunoprecipitation (IP) of ZO-1 with either claudin-5, occludin, JAM-A or β-actin showed close association of claudin-5, occludin, JAM-A and β-actin with ZO-1 in control cells and diminished or completely lost interaction in CCM3-KD cells. Western blotting image is one of three independent experiments. Input represents the 50 % of total cell extract used for immunoprecipitation

addition, there was diminished interaction between ZO-1 and actin filaments in CCM3-KD cells (Fig. 3e), which is supported by a detectible alteration in the distribution of ZO-1 in the actin cytoskeleton fraction (Fig. 3e).

These data indicate that reducing CCM3 in brain endothelial cells affects TJ complex organization by changing transmembrane protein:scaffolding protein and scaffolding protein:actin cytoskeleton interactions. This, in turn, may affect brain endothelial barrier properties (e.g., hyperpermeability to small molecular weight tracers) and may represent a solid substrate for developing CCM3-type lesions.

CCM3 targets cortactin expression and function at the tight junction complex

Cortactin was the most affected protein in the CCM3 brain tissue analysis (Figs. 1, 2). Thus, we further analyzed cortactin protein and mRNA expression in CCM3-KD brain endothelial cells. CCM3 depletion increased cortactin mRNA expression ($p < 0.05$) but cortactin protein was significantly down-regulated ($p < 0.001$; Fig. 4a, b). These results are similar to those from the patients with CCM3 lesions. In controls, cortactin was present in the cell cytosol and on the border of brain endothelial cells and colocalized with ZO-1 (Fig. 4c). However, CCM3 knockdown led to the disappearance of cortactin from the brain endothelial cell border while the cytosolic portion was still present (Fig. 4c).

Altered cortactin localization was further examined by cell fractionation. In control cells, cortactin was mostly present in the membrane and actin cytoskeletal fractions, resembling the finding from immunofluorescence. In CCM3-KD cells, cortactin was mostly redistributed between the cytosol and actin cytoskeleton fractions (Fig. 4d). Due to the close association of cortactin with the actin cytoskeleton fraction in cell cytosol and membrane (cortical actin ring), we isolated two Triton-insoluble fractions: high density (HD), which has high accumulation of cytosolic actin filaments, and low density (LD), which predominantly contains membrane-associated actin filaments. In control cells, cortactin was predominantly found in the membrane actin fraction (low-density Triton-insoluble fraction) and the cytosol actin cytoskeleton fraction (high-density Triton-insoluble fraction) (Fig. 4d). However, in CCM3-KD cells, there was a shift of cortactin from the low- and high-density Triton-insoluble fractions to the cytosol fraction (Triton-soluble fraction), with complete absence from membrane actin cytoskeleton fraction and decreased presence in the actin cytoskeleton fraction (Fig. 4d). This redistribution of cortactin was further associated with a loss of colocalization/interaction between cortactin and ZO-1, as well as cortactin with actin filaments (Fig. 4e).

A potential role of cortactin in the barrier hyperpermeability with CCM3-KD cells was confirmed in rescue experiments where CCM3 cDNA was added to CCM3-KD cell (with efficiency of expression of 50 % for mRNA or 41 % for CCM3 protein). Adding CCM3 to CCM3-KD cells partially reestablished cortactin protein expression in CCM3-KD cells (Fig. 4f) and reduced the CCM3-KD monolayer permeability to 5 kDa inulin (day 5 of initial plating: $PC_{CCM3\text{-}KD} = 5.43 \pm 0.78 \times 10^{-4}$ cm/min compared to $PC_{CCM3\text{-}KD+CCM3} = 3.43 \pm 0.31 \times 10^{-4}$ cm/min, $p < 0.01$; Fig. 4g). Thus, CCM3 could be involved in regulating TJ complex stability and barrier permeability by regulating
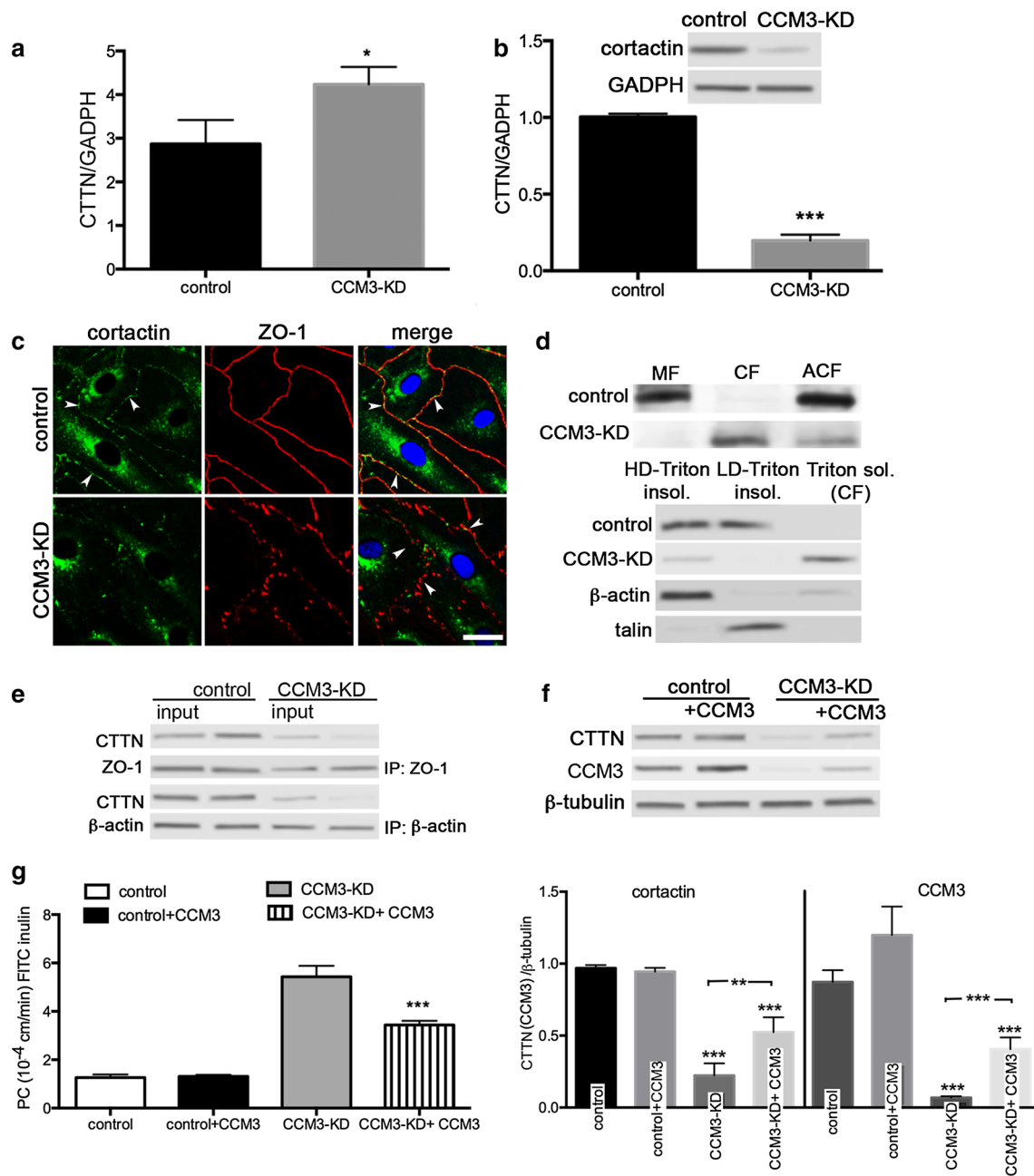
cortactin expression in brain endothelial cells, suggesting cortactin is a major target for the dysfunctional of TJ complex in CCM3 lesions.

CCM3 KD-induced cortactin depletion is mediated by proteasome degradation

The difference between the effects of CCM3-KD on cortactin mRNA (increased) and protein (decreased) expression suggested a potential effect on cortactin protein turnover. This was examined by comparing cortactin protein expression in control and CCM3-KD cells in the presence of

cycloheximide (CXD) for 3–24 h to inhibit de novo cortactin synthesis. Cortactin in CCM3-KD cells had accelerated degradation, with a half-life of 3 h compared to 6 h in control cells (Fig. 5a). In addition, treating CCM3-KD and control cells with the transcription inhibitor actinomycin D did not alter cortactin expression (data not shown) indicating that CCM3 is directly involved in regulating cortactin protein expression at the post-transcriptional level (Fig. 5a).

To examine the mechanism of cortactin degradation, CCM3-KD and control cells were treated with CXD for 3–24 h in the presence either a proteasome (MG-132) or a lysosomal (leupeptin) inhibitor. MG-132, but not leupeptin,

Fig. 4 a, **b** Real-time RT-PCR and Western blot analysis of cortactin (CTTN) expression in control and CCM3-KD cells showed higher cortactin mRNA expression in CCM3-KD cells but significantly decreased protein levels. mRNA and protein levels are presented as expression relative to GAPDH, an internal control. Data represent mean $\pm$ SD, $n = 3$; *$p < 0.05$, ***$p < 0.001$ between control and CCM3-KD cells. Western blot image is one of three independent experiments. **c** Cortactin expression was examined by double label immunofluorescence with ZO-1 in control and CCM3-KD cells. Cortactin staining was present in control cells in cell cytosol and as continuous staining at cell borders associated with ZO-1. In CCM3-KD cells, cortactin staining completely disappeared from the cell border. *Scale bar* 20 μm. **d** The initial cell fractionation and Western blot analysis of cortactin distribution showed cortactin present in the membrane (MF) and actin cytoskeleton fraction (ACF) in control cells, while CCM3-KD cells had a redistribution of cortactin to the cytosol (CF) and actin cytoskeleton fraction (ACF). Additional analysis of the actin cytoskeleton fraction by fractionation into high-density Triton100X insoluble (HD-Triton insol) and low-density Triton100X insoluble (LD-Triton insol) fractions. Cortactin presence in the membrane actin cytoskeleton (LD-Triton insol) and cytoplasmic actin (HD-Triton insol) fractions was diminished in CCM3-KD cells compared to control cells. Western blot image is one of three independent experiments. **e** Co-immunoprecipitation of either ZO-1 or β-actin with cortactin showed close association of cortactin with ZO-1 and β-actin in control cells and diminished or completely lost interaction in CCM3-KD cells. Western blot image is one of three independent experiments. Input represents the 50 % of total cell extract used for immunoprecipitation. **f** Rescuing of CCM3-KD cells with CCM3 cDNA restored both CCM3 and cortactin protein expression. Western blot image is one of three independent experiments. Semi-quantitative densitometry for cortactin and CCM3 protein expression was performed and normalized to β-tubulin as an internal control in five independent experiments. Graph represents mean $\pm$ SD, $n = 5$; **$p < 0.01$, ***$p < 0.001$ comparing control and CCM3-KD cells and CCM3-KD and CCM3-KD + CCM3 cells, respectively. **g** It also improved brain endothelial barrier integrity in CCM3-KD cells with decreased permeability to FITC-Inulin. Graph represents mean $\pm$ SD, $n = 3$; ***$p < 0.001$

blocked cortactin degradation in both control and CCM3-KD cells pinpointing that proteasome pathway as the one involved in cortactin turnover and the degradation induced by CCM3-KD (Fig. 5b). Furthermore, prior to degradation, cortactin underwent ubiquitination and inhibiting that process with SMER3 also reduced cortactin depletion in CCM3-KD cells (Fig. 5c). Thus, treating CCM3-KD cells with MG-132 or SMER3 increased cortactin protein levels up to twofold (Fig. 5d). MG-132 also reduced the permeability of CCM3-KD monolayers to inulin-FITC (Fig. 5e). These results indicate that reduced CCM3 accelerates cortactin degradation via the proteasomal–ubiquitination pathway, which in turn affects TJ stability.

Cortactin modification in condition of CCM3 depletion

Cortactin appearance in the cytosolic fraction of CCM3 KD cells and consequent degradation indicate that it might be in a dysfunctional form, which could trigger ultimate degradation. Thus, further analysis focused on the "status"

of cytosolic cortactin in CCM3-KD cells. We first analyzed the kinetics of cytosolic cortactin accumulation during CCM3 depletion. The progressive loss of CCM3 from 1 to 5 days after siRNA transfection was associated with increased cortactin accumulation in the cytosolic fraction (Supplemental Fig. 1; Fig. 6a). Due to the importance of phosphorylation in cortactin function, phosphorylation status was examined in all isolated cell fractions in CCM3-KD and control cells by immunoprecipitation with cortactin antibody and blotting with pan phospho-serine, -threonine or -tyrosine antibodies. Cortactin accumulation in the cytosolic fraction with CCM3-KD was predominantly associated with increased cortactin phosphorylation on Ser residues (Fig. 6a) but not Tyr or Thr residues (data not shown). Cortactin phosphorylation on Tyr residues was mostly associated with the actin cytoskeleton (high-density Triton fraction) and membrane (low density) fraction of cortactin in control cells, while CCM3-KD decreased Tyr-phosphorylated cortactin in both those fractions (Fig. 6a).

Control cells contained very low levels of pS405 phospho-cortactin in the cell cytosol while in CCM3-KD cells at day 5 after transfection and retransfection there was increased accumulation pS405-cortactin evaluated by both Western blot and immunofluorescence (Fig. 6b). Rescuing CCM3 in CCM3-KD cells decreased the accumulation of pS405 phospho-cortactin in cell cytosol (Fig. 6b). The pS405-cortactin was not associated with either ZO-1 or β-actin suggesting that pS405-cortactin has an afunctional role in sealing or stabilizing the brain endothelial cell TJ complex (data not shown). There was no phospho-Tyr421 cortactin in the cell cytosol fraction (data not shown) in CCM3-KD cells. Overexpressing cortactin in CCM3-KD cells increased total cortactin protein levels and slightly increased cortactin association ZO-1 and β-actin (Fig. 6b). Importantly, overexpressing cortactin in these cells improved brain endothelial barrier integrity as measured as with inulin (PC $_{CCM3-KD}$ = 6.06 $\pm$ 0.75 $\times$ 10^{-4} vs. PC $_{CCM3-KD-CTTN}^{over}$ = 3.48 $\pm$ 0.86 $\times$ 10^{-4} cm/min; $p < 0.01$; Fig. 6d). This suggests that cortactin is one target for CCM3 and its loss could be marker of barrier instability in CCM3 lesions.

The phosphorylation on Ser residues pinpointed that loss of CCM3 might trigger the activity of some Ser kinases. Based on prior studies [28, 29, 76], Erk1/2 is linked to phosphorylation of cortactin serine residues. On the other hand, CCM molecules, and particularly CCM2, are involved in regulating RhoA and ROCK activity in endothelial cells and Rho kinase is overactive with mutated/dysfunctional CCM2. Therefore, ERK1/2, RhoA and ROCK activity was analyzed in CCM3-KD cells. CCM3-KD caused long-lasting activation of ERK1/2 (Fig. 7a) but very low activity of RhoA and ROCK I (Supplemental Fig. 2a and b). The direct involvement of ERK1/2 in altering cortactin
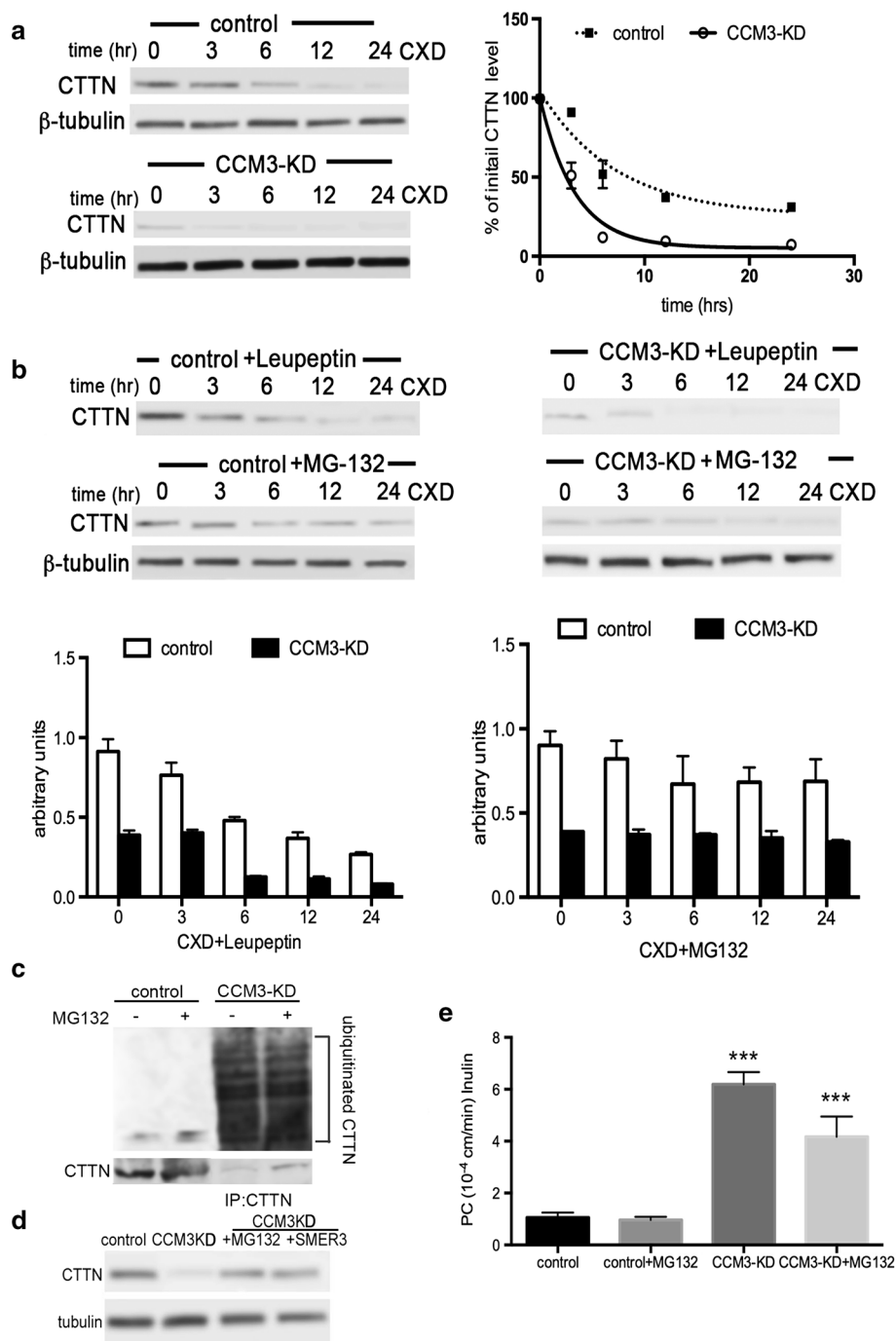
Fig. 5 a Cortactin (CTTN) protein turnover rate was analyzed following treatment with cycloheximide (CXD) in CCM3-KD and control cells. Semi-quantitative densitometry for cortactin was performed using β-tubulin as internal control. Cycloheximide (5 μg/ml) was added for 0–24 h. Time point 0 is start for CXD treatment and for control and CCM3-KD cells was taken as 100 % cortactin expression. The half-life of cortactin was in 5.0 h in controls ($R^2 = 0.916$) and 2.3 h in CCM3-KD cells ($R^2 = 0.972$). Cortactin in CCM3-KD cells had a decreased half-life compared with control cells. **b** Cortactin degradation in control and CCM3-KD cells was also examined in the presence of leupeptin (25 μM), an inhibitor of lysosomal enzymes, or MG-132 (10 μM), an inhibitor of proteasome activity, during treatment with CXD. Representative Western blot images and semi-quantitative densitometry (*graph*) showed that inhibition of protea-some activity by MG132 prevented cortactin degradation in both control and CCM3-KD cells and abolished the difference in degradation between the two types of cells. In contrast, leupeptin did not affect cortactin degradation in either cell type. Graphs show mean ± SD, $n = 3$ independent experiments. **c** The ubiquitination of cortactin (CTTN) in control and CCM3-KD cells was detected by Western blot using anti-ubiquitin antibody. **d** Cortactin protein expression in CCM3-KD cells was rescued by inhibiting proteasome activity with MG132 or by treatment with the ubiquitin E3 ligase inhibitor SMER3 (50 μM). Western blot image is one of three independent experiments. **e** Permeability coefficient (PC) for FITC-inulin in CCM3-KD and control cells after treatment with the proteasome inhibitor MG132. Data represent means ± SD for $n = 3$ independent experiments, ***$p < 0.001$
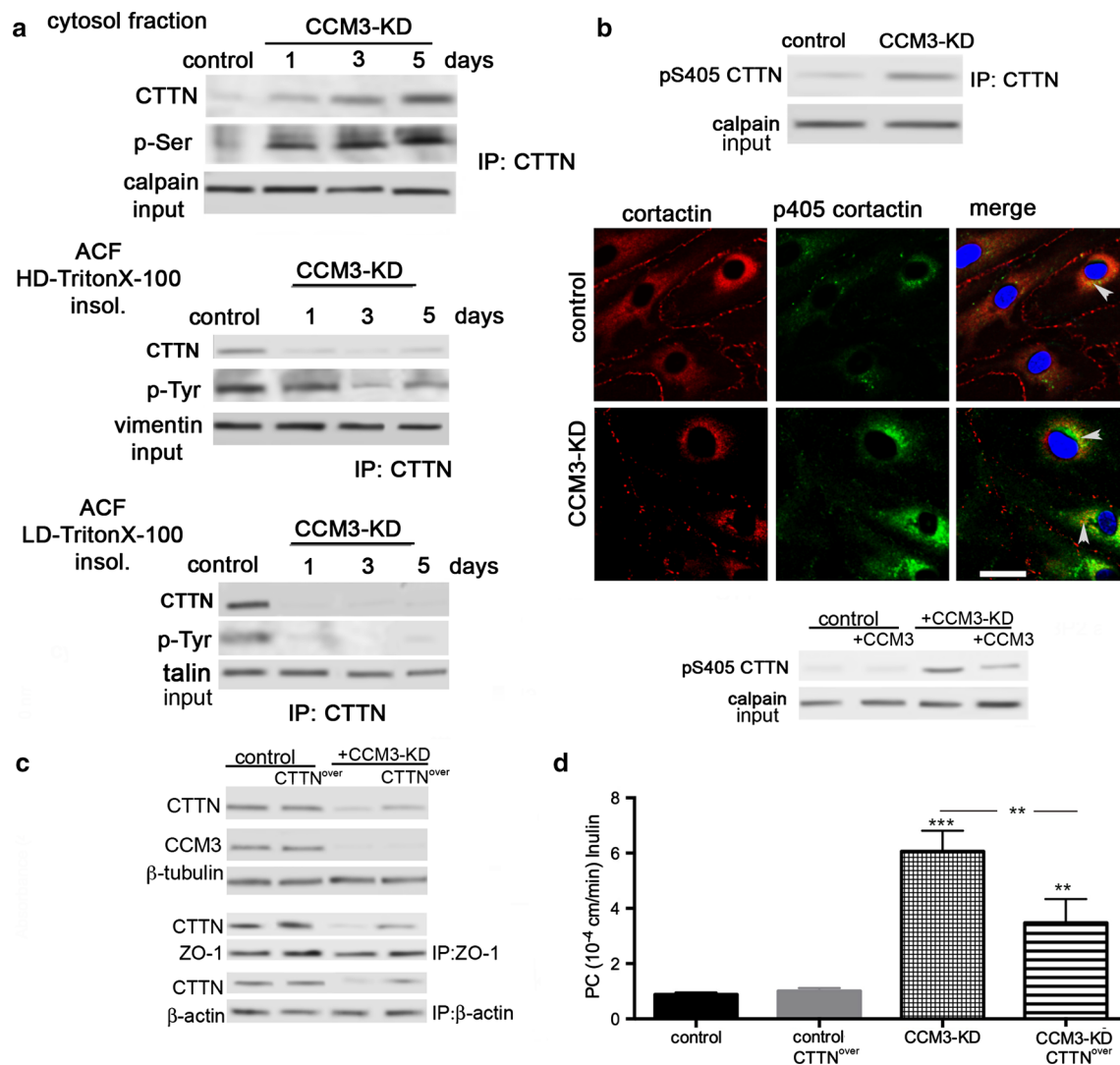
Fig. 6 a Phosphorylation status of cortactin in control and CCM3-KD cells. Western blot analysis of the cytosol (triton-soluble fraction) and both actin cytoskeleton fractions, low-density TritonX-100 insoluble (membrane) and high-density TritonX-100 insoluble actin cytoskeleton (cytosol) fractions, showed increased serine phosphorylation (p-Ser) of cortactin in the cytosol fraction in CCM3-KD cells while tyrosine phosphorylation (p-Tyr) was depleted in both actin cytoskeleton fractions. Western blot image is one of three independent experiments for 1–5 days after CCM3 siRNA transfection. b Representative images of immunofluorescence and Western blot analysis of cortactin in CCM3-KD and control cells showed accumulation of p-Serine405 (pS405) phosphorylated cortactin in CCM3-KD cells in cytosol fraction (calpain + fraction). Rescuing CCM3 in CCM3-KD cells decreased the p-Serine405 (pS405) cortactin. Western blot image is one of three independent experiments. c Cortactin overexpression in CCM3-KD cells (CTTN^{over}) rescued the expression of cortactin. Western blot analysis indicated the cortactin presence in CCM3-KD cells at day 1 after transfection. The overexpression of cortactin also lead to establish the cortactin-ZO-1 and cortactin-β-actin interaction in CCM3-KD cells indicating that rescuing cortactin may improve the cortactin availability for "physiological" function. Western blot image is one of three independent experiments. d Overexpression of cortactin in CCM3-KD cells also improved brain endothelial barrier integrity with decreased permeability to FITC-inulin. Graph represents means ± SD, $n = 3$; ***$p < 0.001$ comparing to control and **$p < 0.01$ comparing CCM3-KD and CCM3-KD CTTN^{over} cells

expression and cortactin S405 phosphorylation was further confirmed using an inhibitor, PD098059, or ERK1/2 siRNA. In both conditions, pS405 cortactin levels were attenuated and cortactin presence in the cytosol (Triton-soluble fraction) was reduced in CCM3-KD brain endothelial cells (Fig. 7b). On the other hand, cortactin expression was increased and shifted towards the membrane (low-density Triton-insoluble) and actin cytoskeletal (high-density Triton-insoluble) fractions. Inhibiting ERK1/2 activity in CCM3-KD cells with PD098059 or ERK1 siRNA also improved barrier integrity with decreased permeability to inulin (Fig. 7c). These results indicate that loss of CCM3,
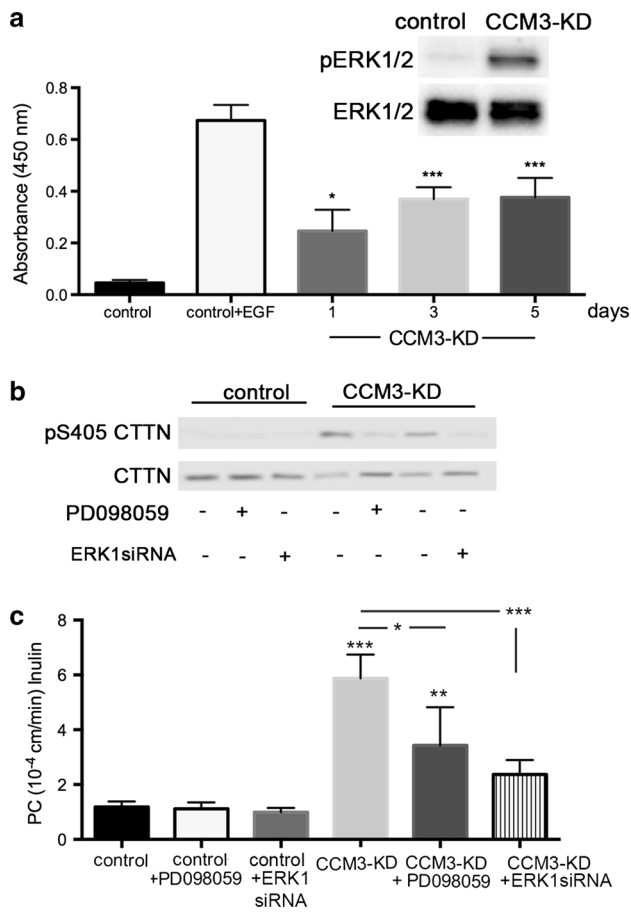
Fig. 7 a CCM3-KD cells showed a steady increased activity of ERK1/2 compared to control cells. ERK1/2 activity was measured by Western blot analysis of phospho-ERK1/2 (Western blot) as well as ERK1/2 activation assay (*graph*). The positive control for ERK1/2 activation was epidermal growth factor (EGF; 10 ng/ml). Data represent an average $\pm$ SD for $n = 3$ independent experiments, $*p < 0.05$, $***p < 0.001$ vs. control cells. **b** Inhibition of ERK1/2 activity either via PD098059 or transient transfection with ERK1 siRNA showed depleted pS405 cortactin in cell cytosol and increased total cortactin expression in CCM3-KD cells. Western blot image is one of three independent experiments. **c** ERK1/2 inhibition either with PD098059 or ERK1/2 siRNA was also associated with stabilization of brain endothelial barrier and decreased permeability to FITC-Inulin. Data represent an average $\pm$ SD for $n = 4$ independent experiments. $*p < 0.05$ vs. no PD098059 treatment, $***p < 0.001$ vs. no ERK1/2 siRNA transfection

by modifying ERK1/2 activity, regulates cortactin function at the TJ complex and, thereby, TJ complex stability and brain endothelial barrier integrity.

Cortactin plays an important role in regulating brain endothelial barrier integrity

Cortactin loss in brain endothelial cells was a common major finding with CCM3 lesions and CCM3-KD cells. Thus, we further investigated how cortactin affects

TJ complex organization in brain endothelial cells. We knocked down cortactin using either shRNA to produce a stable cell line or by transient transfection with cortactin shRNA. Both types of knockdown depleted cortactin between 65–95 % (Fig. 8a). Loss of cortactin significantly affected brain endothelial barrier integrity, with increased permeability for inulin (5 kDa) and dextran (20 and 40 kDa). As shown in Fig. 8a, cortactin-KD cells did not establish complete endothelial barrier integrity after initial plating, showing a steady increased permeability compared to control (mock) transfected cells for the small molecular tracer, inulin 5 kDa (day 7 PC$_{CTTNKD}$ = 6.5 $\pm$ 0.14 $\times$ 10^{-4}; control PC$_{control}$ = 0.04 $\pm$ 0.03 $\times$ 10^{-4} cm/min, $p < 0.001$). There was also a slower establishment of impermeability to 20 kDa dextran with cortactin-KD (e.g., at day 7: PC$_{CTTNKD}$=0.63 $\pm$ 0.13 $\times$ 10^{-4} vs. PC$_{control}$ = 0.07 $\pm$ 0.03 $\times$ 10^{-4} cm/min; $p < 0.05$; Fig. 8a). Cortactin-KD and control cells did not show significant differences in permeability to 40 kDa dextran (data not shown).

Analysis of TJ complex organization in cortactin-KD cells compared to control cells indicated that claudin-5 and occludin staining on the lateral membrane was discontinuous with both proteins also appearing in the cytosol (Fig. 8b). Furthermore, ZO-1 showed more frequent zigzag structure with cortactin depletion and increased punctate staining not seen in control cells (Fig. 8b). There were marked actin cytoskeleton alterations with cortactin-KD. The cortical actin ring structure was lost and there was formation of short stress fibers (Fig. 8b). Analysis of the TJ protein interaction indicated that cortactin-KD cells had decreased to complete loss of claudin-5:ZO-1, occludin:ZO-1 as well as ZO-1:actin filament interactions. These results pinpoint that cortactin plays a role in TJ complex organization and the establishment of essential protein–protein interactions (Fig. 8c).

Taking into consideration results from CCM3-KD and cortactin-KD cells and the similar alterations at the TJ complex, CCM3 may regulate brain endothelial barrier integrity by altering the functional status and presence of cortactin at the TJ complex. Diminished cortactin expression, mutation or loss of CCM3 may affect TJ complex stability and alter essential TJ protein interactions. This could represent a solid substrate for developing the CCM3 lesion.

Discussion

The present study aimed to establish the role of CCM3 in regulating brain endothelial barrier integrity and potential targets of CCM3 action at the TJ complex. We found that: (a) CCM3 regulates brain endothelial barrier integrity and TJ complex organization. (b) One target of CCM3 is the actin-binding protein cortactin, a part of the cortical actin
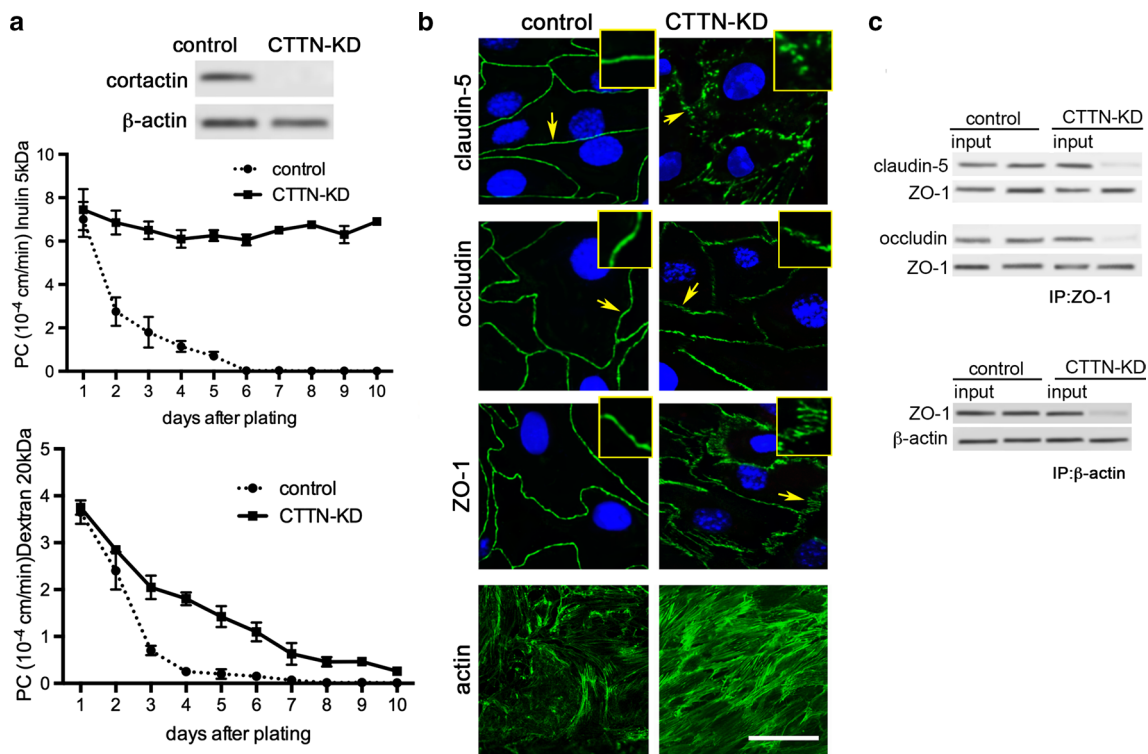
Fig. 8 **a** Stable transfection with cortactin shRNA (CTTN-KD) in hBMEC depleted cortactin (Western blot) and increased endothelial barrier permeability (a similar effect as CCM3-KD). The permeability of FITC-inulin (5 kDa) and dextran (20 kDa) was measured 1–10 days after initial plating in CTTN-KD and control transfected brain endothelial monolayers and a permeability coefficient (PC) determined. In control cells, the permeability of FITC-inulin and dextran progressively declined with time. In contrast, with CTTN-KD cells, the reduction in dextran permeability was delayed and incom-plete over 10 days, while for inulin the permeability did not decrease with time. Data are means SD; $n = 5$ independent experiments. **b** CTTN-KD cells had altered TJ protein immunofluorescence mani-fested as fragmented staining for claudin-5, occludin and ZO-1 and robust short stress fiber formation visualized by phalloidin staining. **c** Co-immunoprecipitation and Western blot analysis showed loss of interaction between ZO-1 with claudin-5 or occludin and β-actin with ZO-1. Western blot image is one of three independent. Input repre-sents the 50 % of total cell extract used for immunoprecipitation

ring, which provides support for essential interactions inside the TJ complex. (c) Loss of CCM3 causes steady activation of MAP kinase ERK1/2 responsible for cortactin phosphorylation and increased degradation. (d) Blocking ERK1/2 in brain endothelial cells prevented TJ complex disassembly and brain endothelial barrier hyperpermeabil-ity with CCM3 depletion.

Before discussing the implications of these findings, a potential technical concern needs to be addressed: using an in vitro model to study the effect of CCM3 mutations in brain endothelial cells. We are aware of the limitations of in vitro studies due to the absence of important perivascular interactions, which could, according to current hypotheses, have significant impact on lesion development. However, CCM3 mutation/absence in brain endothelial cells repre-sents one component important for lesion development and presumably all CCM genes, including CCM3, have effects on brain endothelial cell phenotype. In addition, there are limitations in CCM3 in vivo models. Both CCM3 knock-out and conditional CCM3 knockout mice do not fully recapitulate human CCM3 [19, 34, 37, 41]. Thus, taking these limitations into consideration, the proposed in vitro model of CCM3 depletion by siRNA in HBMEC may still resemble the ongoing molecular mechanisms altering the brain endothelial barrier and endothelial phenotype in CCM3 pathogenesis.

Cerebral cavernous malformation lesions are lined by brain endothelial cells characterized by poorly formed TJs with gaps often noted between individual cells [5, 6, 23, 50]. Although this represents a developed lesion, the cur-rent hypothesis is that microvascular hyperpermeability is a solid base for the development of all CCMs [3, 8, 16, 39, 73]. It results in a common pathological substrate, accu-mulation of blood-borne compounds in brain parenchyma, inflammatory responses, and further endothelial injury which can lead to lesion progression [6, 14, 16, 53].

The brain microvasculature has unique organization properties due to the development of a highly restrictive and selective barrier that controls exchange between blood and brain, the BBB. The unique restrictive feature of the

BBB results from a well-developed junctional complex, particularly the TJs, that completely occlude the brain endothelial paracellular space [57]. TJ complex is built on intricate interactions between transmembrane TJ proteins (claudin-5, occludin, JAM-A), scaffolding proteins (ZO-1, -2, -3, Af-6, VASP, Par3, Par6) and the actin cytoskeleton [40, 42, 64]. Of the transmembrane proteins, claudin-5 forms the primary TJ seal, while occludin and JAM-A regulate paracellular permeability and leukocyte migration, respectively [11, 42, 64]. The TJ accessory proteins are multidomain cytoplasmic molecules, which structurally support the TJ (ZO-1, -2, -3) as well as being involved in signal transduction (cingulin, 7H6 and atypical protein kinase C) [38, 47]. In addition, actin filaments extend into the TJs (linked to ZO-1 and occludin), coupling the structural and dynamic properties of the paracellular barrier. To obtain a tightly sealed TJ, trans-interactions between transmembrane TJ proteins (particularly claudin-5) are essential as well as stable support/interaction with adaptor proteins (ZO-1, -2) and actin filaments [15, 65]. In this way, the TJ junction complex acts as a dynamic structure and alterations in the function of any of these components may lead to paracellular gap formation and barrier hyperpermeability [57, 65].

A major pathological sign of increased BBB permeability is altered transmembrane TJ protein expression (i.e., claudin-5 and occludin) demonstrated as lost or fragmented staining along blood vessels or the lateral border of cultured brain endothelial cells [54, 58]. For CCM lesions, known for high permeability, pathological findings regarding altered TJ protein expression are very controversial, with results varying from increased expression of some TJ proteins, decreased expression of others (i.e., claudin-5, occludin) and very limited alterations in yet others [5, 6, 23, 50, 61]. These mixed results could be due to analysis of lesions of different maturity and size but also differences in the origin of analyzed lesions (e.g., CCM1, CCM2 CCM3 or sCCM). This study focused on the expression profile of TJ and AdJ proteins in two types of CCM lesion: CCM3 and sCCM. Both TJ and AdJ mRNA and protein showed a similar expression pattern in CCM3 and sCCM with upregulation of mRNA expression and down-regulation in protein expression while decreased TJ protein expression was more profound in CCM3 lesions, particularly for transmembrane TJ protein which may be linked to the CCM3 mutation. However, the tendency for both lesion types to have reduced junction protein expression indicates that besides a direct link between CCM3 and junction proteins there could be parallel effects in endothelial cells and from the perivascular microenvironment, which could support lesion formation.

Taking into consideration that CCM3 is a more severe form of CCM, with higher frequency of hemorrhage at earlier ages, the profound effect CCM3 mutation on TJ complex organization could represent the underlying cellular mechanism of microvascular damage seen in CCM3 [12, 46]. The mechanism underlying the loss of claudin-5, occludin and ZO-1 with CCM3 depletion/loss is still uncertain and future studies need to examine the effect of CCM3 on the translation and post-translational modification of these TJ proteins.

Regarding the potential targets and overlap with CCM1 and CCM2 pathology, in our current study CCM3 lesion and CCM3-KD cells did not have the significant alterations in the AdJ proteins, β-catenin and Ve-cadherin found in CCM1 or alterations in RhoA/Rho kinase activity specific for CCM2 pathology [17, 33, 49, 59]. This indicates that CCM1, CCM2 and CCM3 probably do not share a similar target at the junctional complex. However, we have still to directly address whether CCM3 in the CCM1-3 complex or in the STRIPAK complex is responsible for altered barrier function [10, 21, 74].

An intriguing finding from this study is that CCM3 mutation/depletion had a profound effect on cortactin protein expression. Cortactin is a 550 amino acid F-actin-binding protein, primarily localized on the circumference of endothelial cells [7, 15, 44]. In recent years, a growing body of evidence has implicated cortactin in multiple aspects of cytoskeletal organization such as lamellipodia, membrane ruffles, endocytosis, actin-based structures in the cell periphery (so-called "cortical actin bundles") and cell–cell junction contact [20, 44, 48, 51]. While the role of cortactin in actin polymerization and maintaining actin cytoskeletal structure has mostly been elucidated, the role at cell–cell junction complexes is still unclear. Cortactin is indicated as having an important role in E-cadherin recruitment and stabilization at the cell membrane, playing a role in establishing initial cell–cell contacts and AdJ formation [18, 20, 55]. Regarding the TJ complex, cortactin function is still uncertain. Cortactin is identified as having a binding site for ZO-1 (SH3 region of cortactin and proline-rich domain of ZO-1) [25, 30, 70]. This provides a structural link between TJ complex proteins (ZO-1) and the actin cytoskeleton that is important for anchoring and reinforcing junctions in endothelial cells [15, 18].

Combining our findings from CCM3- and cortactin-KD cells indicates that loss of cortactin reduces ZO-1 interaction with the actin cytoskeleton, which could cause less anchoring of the TJ to the cytoskeleton. Loss of cortactin was also associated with profound changes in the cytoskeleton itself with dissolution of the cortical actin ring and increased polymerization of the actin cytoskeleton. Loss of ZO-1 anchoring could affect the TJ interactions between ZO-1 and the transmembrane proteins claudin-5 and occludin [11]. This could weaken the adhesive properties between claudin-5 on neighboring endothelial

cells and probably, consequently, claudin-5 redistribution towards to cytosol. Our finding regarding claudin-5, ZO-1 and occludin redistribution to the cytosol and loss of interaction when cortactin is depleted/absent favors this scenario. However, we do not exclude the possibility that during TJ disassembly, cortactin loss and cortical actin ring dissolution could trigger dysregulation of signaling molecules associated with cortactin (like Rac and RacGEF) by which cortactin may act as a stabilizing factor for the actin cytoskeleton and cell–cell junctions [68, 75].

An arising question is the potential link between CCM3 absence/mutation and the cortactin depletion found in brain endothelial cells. Cortactin function is highly dependent on post-translation modification and particularly phosphorylation. For example, cortactin phosphorylation on Tyr residues (Tyr^{421}, Tyr^{466}, Tyr^{482}) is essential for several actin-based processes including podosomal formation, lamellipodial protrusion, cell spreading, cell motility, intercellular adhesion (E-cadherin and β-catenin) and also in adhesion molecule clustering during leukocyte transmigration [29, 62, 67, 69]. Cortactin Ser-phosphorylation facilitates cortactin binding to N-WASP and actin polymerization [28, 29, 76]. On the other hand, a cytosolic cortactin pool is unphosphorylated and can, when stimulated, translocate to cortical actin and take part in cell processes. Our analysis of CCM3-KD cells indicated that CCM3 depletion caused an accumulation of cortactin in the cell cytosol, not in the unphosphorylated form but rather as Ser-phosphorylated (p-S405) cortactin, dissociated from ZO-1 and the actin cytoskeleton [28, 36]. The increased accumulation of p-S405 cortactin in the cytosol is further subjected to proteasomal degradation, indicating that CCM3 by regulating cortactin phosphorylation regulates cortactin function and stability in brain endothelial cells. This was closely associated with the increased of ERK1/2 activity in CCM3-KD cells, one of the serine/threonine kinases involved in regulating cortactin function via serine phosphorylation [70, 76]. CCM3 depletion caused steady moderate ERK1/2 activity, which may directly phosphorylate cortactin on

Ser405 residues leading to the enhanced brain endothelial barrier permeability seen in CCM3-KD cells, as found in an epithelial barrier after treatment with LPS, where ERK1/2 phosphorylation increased cortactin phosphorylation and degradation via ubiquitination, the potential pathway also present in CCM3-KD cells [76]. At this point, we cannot conclude whether pS405-cortactin is a unique marker for altered CCM3 expression/function in brain endothelial cells and exclude that other cortactin Ser-phosphorylation sites are involved in CCM3. The pS405-cortactin in CCM3-KD cells could be one of consequence of steady ERK/12 activity and further analysis of phosphorylation status of cortactin as well as the role of specific phosphorylated residues of cortactin in CCM3 lesion should clarify this issue. Further analysis should include whether the cytosol-accumulated phosphorylated form of cortactin is the one important for ubiquitination and proteasomal degradation [76].

Taken together, the results presented here suggest a potential scenario triggering CCM3 lesion formation (Fig. 9). Loss of CCM3 triggers or chronically maintains ERK1/2 activation. This in turn alters actin cytoskeleton organization by targeting, among others, the cortical actin ring protein cortactin by inducing Ser-phosphorylation. This changes both cortactin location and degradation. Increased cortactin degradation is closely associated with loss of the cortical actin ring and ZO-1:actin interaction, two essential components providing physical support and anchoring for TJ proteins. The reduced anchoring of ZO-1 to the actin cytoskeleton may then impact critical interactions between this important scaffolding protein and transmembrane proteins in the TJ complex, altering their function. In addition, increased polymerization of actin filaments due to loss of cortactin may increase intracellular forces causing TJ instability. These events could represent the mechanism underlying increased BBB permeability in CCM3 lesions. It is important to highlight that during CCM3 lesion formation, the described process would lead to parenchymal entry of blood-borne components further fueling barrier disruption.

Fig. 9 Possible scenario of the signaling events induced by CCM3 mutation/depletion in brain endothelial cells that result in tight junction complex instability and brain endothelial barrier hyperpermeability
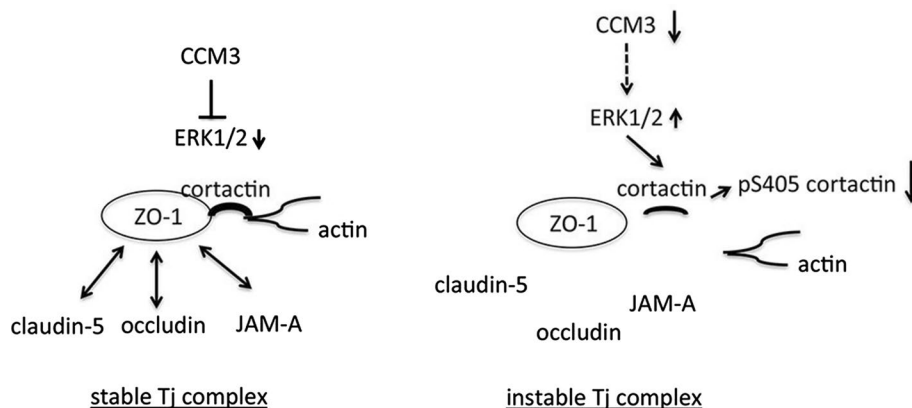
Besides describing the potential cellular mechanism underlying the hyperpermeability in CCM3 lesions, our results also reveal that a signaling pathway other than RhoA/ROCKI may be involved in CCM lesions: MAP kinase ERK1/2. Due to the pivotal role of this pathway in cell homeostasis, it is impossible to exclude that steady-active ERK1/2 activation does not regulate other brain endothelial phenotype changes found in CCM3, including the process of endothelial to mesenchymal transformation recently indicated as one mechanism underlying CCM3 lesion progression [35]. Our results also provide a solid basis for further investigation of the potential link between CCM3 and ERK1/2 activation to develop an efficient therapeutic strategy for targeting the hyperpermeability in CCM3 lesions.

References

1. Afridi S, Goadsby PJ (2003) New onset migraine with a brain stem cavernous angioma. J Neurol Neurosurg Psychiatry 74:680–682

2. Al-Shahi Salman R (2012) The outlook for adults with epileptic seizure(s) associated with cerebral cavernous malformations or arteriovenous malformations. Epilepsia 53(Suppl 4):34–42. doi:10.1111/j.1528-1167.2012.03611.x

3. Awad IA (2012) Cavernous malformations. J Neurosurg 116:119–120. doi:10.3171/2011.6.JNS111052 **(discussion 121)**

4. Borikova AL, Dibble CF, Sciaky N, Welch CM, Abell AN, Bencharit S, Johnson GL (2010) Rho kinase inhibition rescues the endothelial cell cerebral cavernous malformation phenotype. J Biol Chem 285:11760–11764. doi:10.1074/jbc.C109.097220

5. Burkhardt JK, Schmidt D, Schoenauer R, Brokopp C, Agarkova I, Bozinov O, Bertalanffy H, Hoerstrup SP (2010) Upregulation of transmembrane endothelial junction proteins in human cerebral cavernous malformations. Neurosurg Focus 29:E3. doi:10.3171/2010.6.FOCUS10125

6. Clatterbuck RE, Eberhart CG, Crain BJ, Rigamonti D (2001) Ultrastructural and immunocytochemical evidence that an incompetent blood-brain barrier is related to the pathophysiology of cavernous malformations. J Neurol Neurosurg Psychiatry 71:188–192

7. Cosen-Binker LI, Kapus A (2006) Cortactin: the gray eminence of the cytoskeleton. Physiology 21:352–361. doi:10.1152/physiol.00012.2006

8. de Champfleur NM, Langlois C, Ankenbrandt WJ, Le Bars E, Leroy MA, Duffau H, Bonafe A, Jaffe J, Awad IA, Labauge P (2011) Magnetic resonance imaging evaluation

9. Dibble CF, Horst JA, Malone MH, Park K, Temple B, Cheeseman H, Barbaro JR, Johnson GL, Bencharit S (2010) Defining the functional domain of programmed cell death 10 through its interactions with phosphatidylinositol-3,4,5-trisphosphate. PLoS One 5:e11740. doi:10.1371/journal.pone.0011740

10. Draheim KM, Li X, Zhang R, Fisher OS, Villari G, Boggon TJ, Calderwood DA (2015) CCM2-CCM3 interaction stabilizes their protein expression and permits endothelial network formation. J Cell Biol 208:987–1001. doi:10.1083/jcb.201407129

11. Fanning AS, Anderson JM (2009) Zonula occludens-1 and -2 are cytosolic scaffolds that regulate the assembly of cellular junctions. Ann N Y Acad Sci 1165:113–120. doi:10.1111/j.1749-6632.2009.04440.x

12. Fauth C, Rostasy K, Rath M, Gizewski E, Lederer AG, Sure U, Zschocke J, Felbor U (2015) Highly variable intrafamilial manifestations of a CCM3 mutation ranging from acute childhood cerebral haemorrhage to late-onset meningiomas. Clin Neurol Neurosurg 128:41–43. doi:10.1016/j.clineuro.2014.10.023

13. Flemming KD, Brown RD, Link MJ (2015) Seasonal variation in hemorrhage and focal neurologic deficit due to intracerebral cavernous malformations. J Clin Neurosci. doi:10.1016/j.jocn.2015.01.007

14. Frischer JM, Pipp I, Stavrou I, Trattnig S, Hainfellner JA, Knosp E (2008) Cerebral cavernous malformations: congruency of histopathological features with the current clinical definition. J Neurol Neurosurg Psychiatry 79:783–788. doi:10.1136/jnnp.2007.132316

15. Garcia-Ponce A, Citalan-Madrid AF, Velazquez-Avila M, Vargas-Robles H, Schnoor M (2015) The role of actin-binding proteins in the control of endothelial barrier integrity. Thromb Haemost 113:20–36. doi:10.1160/TH14-04-0298

16. Gault J, Sarin H, Awadallah NA, Shenkar R, Awad IA (2004) Pathobiology of human cerebrovascular malformations: basic mechanisms and clinical relevance. Neurosurgery 55:1–16 **(discussion 16–17)**

17. Glading A, Han J, Stockton RA, Ginsberg MH (2007) KRIT-1/CCM1 is a Rap1 effector that regulates endothelial cell cell junctions. J Cell Biol 179:247–254. doi:10.1083/jcb.200705175

18. Han SP, Gambin Y, Gomez GA, Verma S, Giles N, Michael M, Wu SK, Guo Z, Johnston W, Sierecki E et al (2014) Cortactin scaffolds Arp2/3 and WAVE2 at the epithelial zonula adherens. J Biol Chem 289:7764–7775. doi:10.1074/jbc.M113.544478

19. He Y, Zhang H, Yu L, Gunel M, Boggon TJ, Chen H, Min W (2010) Stabilization of VEGFR2 signaling by cerebral cavernous malformation 3 is critical for vascular development. Sci Signal 3:ra26 doi:10.1126/scisignal.2000722

20. Helwani FM, Kovacs EM, Paterson AD, Verma S, Ali RG, Fanning AS, Weed SA, Yap AS (2004) Cortactin is necessary for E-cadherin-mediated contact formation and actin reorganization. J Cell Biol 164:899–910. doi:10.1083/jcb.200309034

21. Hilder TL, Malone MH, Bencharit S, Colicelli J, Haystead TA, Johnson GL, Wu CC (2007) Proteomic identification of the cerebral cavernous malformation signaling complex. J Proteome Res 6:4343–4355. doi:10.1021/pr0704276

22. Hwang J, Pallas DC (2014) STRIPAK complexes: structure, biological function, and involvement in human diseases. Int J Biochem Cell Biol 47:118–148. doi:10.1016/j.biocel.2013.11.021

23. Jakimovski D, Schneider H, Frei K, Kennes LN, Bertalanffy H (2014) Bleeding propensity of cavernous malformations: impact of tight junction alterations on the occurrence of overt hematoma. J Neurosurg 121:613–620. doi:10.3171/2014.6.JNS132775

24. Jensen EC (2013) Quantitative analysis of histological staining and fluorescence using ImageJ. Anat Rec 296:378–381. doi:10.1002/ar.22641

25. Katsube T, Takahisa M, Ueda R, Hashimoto N, Kobayashi M, Togashi S (1998) Cortactin associates with the cell-cell junction protein ZO-1 in both *Drosophila* and mouse. J Biol Chem 273:29672–29677

26. Kazakoff PW, McGuire TR, Hoie EB, Cano M, Iversen PL (1995) An in vitro model for endothelial permeability: assessment of monolayer integrity. In Vitro Cell Dev Biol Anim 31:846–852. doi:10.1007/BF02634568

27. Kean MJ, Ceccarelli DF, Goudreault M, Sanches M, Tate S, Larsen B, Gibson LC, Derry WB, Scott IC, Pelletier L et al (2011) Structure-function analysis of core STRIPAK Proteins: a signaling complex implicated in Golgi polarization. J Biol Chem 286:25065–25075. doi:10.1074/jbc.M110.214486

28. Kelley LC, Hayes KE, Ammer AG, Martin KH, Weed SA (2010) Cortactin phosphorylated by ERK1/2 localizes to sites of dynamic actin regulation and is required for carcinoma lamellipodia persistence. PLoS One 5:e13847. doi:10.1371/journal.pone.0013847

29. Kelley LC, Hayes KE, Ammer AG, Martin KH, Weed SA (2011) Revisiting the ERK/Src cortactin switch. Commun Integr Biol 4:205–207. doi:10.4161/cib.4.2.14420

30. Kremerskothen J, Stolting M, Wiesner C, Korb-Pap A, van Vliet V, Linder S, Huber TB, Rottiers P, Reuzeau E, Genot E et al (2011) Zona occludens proteins modulate podosome formation and function. FASEB J 25:505–514. doi:10.1096/fj.10-155598

31. Krisht KM, Whitehead KJ, Niazi T, Couldwell WT (2010) The pathogenetic features of cerebral cavernous malformations: a comprehensive review with therapeutic implications. Neurosurg Focus 29:E2. doi:10.3171/2010.6.FOCUS10135

32. Labauge P, Denier C, Bergametti F, Tournier-Lasserve E (2007) Genetics of cavernous angiomas. Lancet Neurol 6:237–244. doi:10.1016/S1474-4422(07)70053-4

33. Lampugnani MG, Orsenigo F, Rudini N, Maddaluno L, Boulday G, Chapon F, Dejana E (2010) CCM1 regulates vascular-lumen organization by inducing endothelial polarity. J Cell Sci 123:1073–1080. doi:10.1242/jcs.059329

34. Louvi A, Chen L, Two AM, Zhang H, Min W, Gunel M (2011) Loss of cerebral cavernous malformation 3 (Ccm3) in neuroglia leads to CCM and vascular pathology. Proc Natl Acad Sci 108:3737–3742. doi:10.1073/pnas.1012617108

35. Maddaluno L, Rudini N, Cuttano R, Bravi L, Giampietro C, Corada M, Ferrarini L, Orsenigo F, Papa E, Boulday G et al (2013) EndMT contributes to the onset and progression of cerebral cavernous malformations. Nature 498:492–496. doi:10.1038/nature12207

36. Martinez-Quiles N, Ho HY, Kirschner MW, Ramesh N, Geha RS (2004) Erk/Src phosphorylation of cortactin acts as a switch on-switch off mechanism that controls its ability to activate N-WASP. Mol Cell Biol 24:5269–5280. doi:10.1128/MCB.24.12.5269-5280.2004

37. McDonald DA, Shenkar R, Shi C, Stockton RA, Akers AL, Kucherlapati MH, Kucherlapati R, Brainer J, Ginsberg MH, Awad IA et al (2011) A novel mouse model of cerebral cavernous malformations based on the two-hit mutation hypothesis recapitulates the human disease. Hum Mol Genet 20:211–222. doi:10.1093/hmg/ddq433

38. McNeil E, Capaldo CT, Macara IG (2006) Zonula occludens-1 function in the assembly of tight junctions in Madin-Darby canine kidney epithelial cells. Mol Biol Cell 17:1922–1932. doi:10.1091/mbc.E05-07-0650

39. Mikati AG, Tan H, Shenkar R, Li L, Zhang L, Guo X, Larsson HB, Shi C, Liu T, Wang Y et al (2014) Dynamic permeability and quantitative susceptibility: related imaging biomarkers in cerebral cavernous malformations. Stroke 45:598–601. doi:10.1161/STROKEAHA.113.003548

40. Mitic LL, Anderson JM (1998) Molecular architecture of tight junctions. Annu Rev Physiol 60:121–142. doi:10.1146/annurev.physiol.60.1.121

41. Pagenstecher A, Stahl S, Sure U, Felbor U (2009) A two-hit mechanism causes cerebral cavernous malformations: complete inactivation of CCM1, CCM2 or CCM3 in affected endothelial cells. Hum Mol Genet 18:911–918. doi:10.1093/hmg/ddn420

42. Paris L, Tonutti L, Vannini C, Bazzoni G (2008) Structural organization of the tight junctions. Biochim Biophys Acta 1778:646–659. doi:10.1016/j.bbamem.2007.08.004

43. Rao RK, Basuroy S, Rao VU, Karnaky KJ Jr, Gupta A (2002) Tyrosine phosphorylation and dissociation of occludin-ZO-1 and E-cadherin-beta-catenin complexes from the cytoskeleton by oxidative stress. Biochem J 368:471–481. doi:10.1042/BJ20011804

44. Ren G, Crampton MS, Yap AS (2009) Cortactin: coordinating adhesion and the actin cytoskeleton at cellular protrusions. Cell Motil Cytoskelet 66:865–873. doi:10.1002/cm.20380

45. Riant F, Bergametti F, Ayrignac X, Boulday G, Tournier-Lasserve E (2010) Recent insights into cerebral cavernous malformations: the molecular genetics of CCM. FEBS J 277:1070–1075. doi:10.1111/j.1742-4658.2009.07535.x

46. Riant F, Bergametti F, Fournier HD, Chapon F, Michalak-Provost S, Cecillon M, Lejeune P, Hosseini H, Choe C, Orth M et al (2013) CCM3 mutations are associated with early-onset cerebral hemorrhage and multiple meningiomas. Mol Syndromol 4:165–172. doi:10.1159/000350042

47. Satoh H, Zhong Y, Isomura H, Saitoh M, Enomoto K, Sawada N, Mori M (1996) Localization of 7H6 tight junction-associated antigen along the cell border of vascular endothelial cells correlates with paracellular barrier function against ions, large molecules, and cancer cells. Exp Cell Res 222:269–274. doi:10.1006/excr.1996.0034

48. Schafer DA (2002) Coupling actin dynamics and membrane dynamics during endocytosis. Curr Opin Cell Biol 14:76–81

49. Schneble HM, Soumare A, Herve D, Bresson D, Guichard JP, Riant F, Tournier-Lasserve E, Tzourio C, Chabriat H, Stapf C (2012) Antithrombotic therapy and bleeding risk in a prospective cohort study of patients with cerebral cavernous malformations. Stroke 43:3196–3199. doi:10.1161/STROKEAHA.112.668533

50. Schneider H, Errede M, Ulrich NH, Virgintino D, Frei K, Bertalanffy H (2011) Impairment of tight junctions and glucose transport in endothelial cells of human cerebral cavernous malformations. J Neuropathol Exp Neurol 70:417–429. doi:10.1097/NEN.0b013e31821bc40e

51. Schnoor M, Lai FP, Zarbock A, Klaver R, Polaschegg C, Schulte D, Weich HA, Oelkers JM, Rottner K, Vestweber D (2011) Cortactin deficiency is associated with reduced neutrophil recruitment but increased vascular permeability in vivo. J Exp Med 208:1721–1735. doi:10.1084/jem.20101920

52. Schulz GB, Wieland E, Wustehube-Lausch J, Boulday G, Moll I, Tournier-Lasserve E, Fischer A (2015) Cerebral cavernous malformation-1 protein controls DLL4-Notch3 signaling between the endothelium and pericytes. Stroke. doi:10.1161/STROKEAHA.114.007512

53. Shenkar R, Venkatasubramanian PN, Zhao JC, Batjer HH, Wyrwicz AM, Awad IA (2008) Advanced magnetic resonance imaging of cerebral cavernous malformations: part I. High-field imaging of excised human lesions. Neurosurgery 63:782–789. doi:10.1227/01.NEU.0000325490.80694.A2 **(discussion 789)**

54. Sladojevic N, Stamatovic SM, Keep RF, Grailer JJ, Sarma JV, Ward PA, Andjelkovic AV (2014) Inhibition of junctional adhesion molecule-A/LFA interaction attenuates leukocyte trafficking

and inflammation in brain ischemia/reperfusion injury. Neurobiol Dis 67:57–70. doi:10.1016/j.nbd.2014.03.010

55. Sousa S, Cabanes D, Bougneres L, Lecuit M, Sansonetti P, Tran-Van-Nhieu G, Cossart P (2007) Src, cortactin and Arp2/3 complex are required for E-cadherin-mediated internalization of *Listeria* into cells. Cell Microbiol 9:2629–2643. doi:10.1111/j.1462-5822.2007.00984.x

56. Stahl S, Gaetzner S, Voss K, Brackertz B, Schleider E, Surucu O, Kunze E, Netzer C, Korenke C, Finckh U et al (2008) Novel CCM1, CCM2, and CCM3 mutations in patients with cerebral cavernous malformations: in-frame deletion in CCM2 prevents formation of a CCM1/CCM2/CCM3 protein complex. Hum Mutat 29:709–717. doi:10.1002/humu.20712

57. Stamatovic SM, Keep RF, Andjelkovic AV (2008) Brain endothelial cell-cell junctions: how to "open" the blood brain barrier. Curr Neuropharmacol 6:179–192. doi:10.2174/157015908785777210

58. Stamatovic SM, Keep RF, Wang MM, Jankovic I, Andjelkovic AV (2009) Caveolae-mediated internalization of occludin and claudin-5 during CCL2-induced tight junction remodeling in brain endothelial cells. J Biol Chem 284:19053–19066. doi:10.1074/jbc.M109.000521

59. Stockton RA, Shenkar R, Awad IA, Ginsberg MH (2010) Cerebral cavernous malformations proteins inhibit Rho kinase to stabilize vascular integrity. J Exp Med 207:881–896. doi:10.1084/jem.20091258

60. Sugden PH, McGuffin LJ, Clerk A (2013) SOcK, MiSTs, MASK and STicKs: the GCKIII (germinal centre kinase III) kinases and their heterologous protein-protein interactions. Biochem J 454:13–30. doi:10.1042/BJ20130219

61. Tanriover G, Sozen B, Seker A, Kilic T, Gunel M, Demir N (2013) Ultrastructural analysis of vascular features in cerebral cavernous malformations. Clin Neurol Neurosurg 115:438–444. doi:10.1016/j.clineuro.2012.06.023

62. Tehrani S, Tomasevic N, Weed S, Sakowicz R, Cooper JA (2007) Src phosphorylation of cortactin enhances actin assembly. Proc Natl Acad Sci 104:11933–11938. doi:10.1073/pnas.0701077104

63. Tu J, Stoodley MA, Morgan MK, Storer KP (2005) Ultrastructural characteristics of hemorrhagic, nonhemorrhagic, and recurrent cavernous malformations. J Neurosurg 103:903–909. doi:10.3171/jns.2005.103.5.0903

64. Van Itallie CM, Anderson JM (2014) Architecture of tight junctions and principles of molecular composition. Semin Cell Dev Biol 36:157–165. doi:10.1016/j.semcdb.2014.08.011

65. Vandenbroucke E, Mehta D, Minshall R, Malik AB (2008) Regulation of endothelial junctional permeability. Ann N Y Acad Sci 1123:134–145. doi:10.1196/annals.1420.016

66. Voss K, Stahl S, Schleider E, Ullrich S, Nickel J, Mueller TD, Felbor U (2007) CCM3 interacts with CCM2 indicating common pathogenesis for cerebral cavernous malformations. Neurogenetics 8:249–256. doi:10.1007/s10048-007-0098-9

67. Wang W, Liu Y, Liao K (2011) Tyrosine phosphorylation of cortactin by the FAK-Src complex at focal adhesions regulates cell motility. BMC Cell Biol 12:49. doi:10.1186/1471-2121-12-49

68. Waschke J, Burger S, Curry FR, Drenckhahn D, Adamson RH (2006) Activation of Rac-1 and Cdc42 stabilizes the microvascular endothelial barrier. Histochem Cell Biol 125:397–406. doi:10.1007/s00418-005-0080-2

69. Webb BA, Jia L, Eves R, Mak AS (2007) Dissecting the functional domain requirements of cortactin in invadopodia formation. Eur J Cell Biol 86:189–206. doi:10.1016/j.ejcb.2007.01.003

70. Weed SA, Karginov AV, Schafer DA, Weaver AM, Kinley AW, Cooper JA, Parsons JT (2000) Cortactin localization to sites of actin assembly in lamellipodia requires interactions with F-actin and the Arp2/3 complex. J Cell Biol 151:29–40

71. Wisniewski JR, Mann M (2012) Consecutive proteolytic digestion in an enzyme reactor increases depth of proteomic and phosphoproteomic analysis. Anal Chem 84:2631–2637. doi:10.1021/ac300006b

72. Wong JH, Awad IA, Kim JH (2000) Ultrastructural pathological features of cerebrovascular malformations: a preliminary report. Neurosurgery 46:1454–1459

73. Yadla S, Jabbour PM, Shenkar R, Shi C, Campbell PG, Awad IA (2010) Cerebral cavernous malformations as a disease of vascular permeability: from bench to bedside with caution. Neurosurg Focus 29:E4. doi:10.3171/2010.5.FOCUS10121

74. Yoruk B, Gillers BS, Chi NC, Scott IC (2012) Ccm3 functions in a manner distinct from Ccm1 and Ccm2 in a zebrafish model of CCM vascular disease. Dev Biol 362:121–131. doi:10.1016/j.ydbio.2011.12.006

75. Zebda N, Tian Y, Tian X, Gawlak G, Higginbotham K, Reynolds AB, Birukova AA, Birukov KG (2013) Interaction of p190RhoGAP with C-terminal domain of p120-catenin modulates endothelial cytoskeleton and permeability. J Biol Chem 288:18290–18299. doi:10.1074/jbc.M112.432757

76. Zhao J, Wei J, Mialki R, Zou C, Mallampalli RK, Zhao Y (2012) Extracellular signal-regulated kinase (ERK) regulates cortactin ubiquitination and degradation in lung epithelial cells. J Biol Chem 287:19105–19114. doi:10.1074/jbc.M112.339507